CHONDRULE FORMATION IN BOW SHOCKS AROUND ECCENTRIC PLANETARY EMBRYOS

Melissa A. Morris[1], Aaron C. Boley[2], Steven J. Desch[1], and Themis Athanassiadou[1]

[1] School of Earth and Space Exploration, Arizona State University, P.O. Box 871404, Tempe, AZ 85287-1404, USA; melissa.a.morris@asu.edu
[2] Department of Astronomy University of Florida, Gainesville, FL 32611, USA

ABSTRACT

Recent isotopic studies of Martian meteorites by Dauphas & Pourmand have established that large ($\sim$3000 km radius) planetary embryos existed in the solar nebula at the same time that chondrules—millimeter-sized igneous inclusions found in meteorites—were forming. We model the formation of chondrules by passage through bow shocks around such a planetary embryo on an eccentric orbit. We numerically model the hydrodynamics of the flow and find that such large bodies retain an atmosphere with Kelvin–Helmholtz instabilities allowing mixing of this atmosphere with the gas and particles flowing past the embryo. We calculate the trajectories of chondrules flowing past the body and find that they are not accreted by the protoplanet, but may instead flow through volatiles outgassed from the planet's magma ocean. In contrast, chondrules *are* accreted onto smaller planetesimals. We calculate the thermal histories of chondrules passing through the bow shock. We find that peak temperatures and cooling rates are consistent with the formation of the dominant, porphyritic texture of most chondrules, assuming a modest enhancement above the likely solar nebula average value of chondrule densities (by a factor of 10), attributable to settling of chondrule precursors to the midplane of the disk or turbulent concentration. We calculate the rate at which a planetary embryo's eccentricity is damped and conclude that a single planetary embryo scattered into an eccentric orbit can, over $\sim$10^5 years, produce $\sim$10^{24} g of chondrules. In principle, a small number (1–10) of eccentric planetary embryos can melt the observed mass of chondrules in a manner consistent with all known constraints.

Key words: instabilities – meteorites, meteors, meteoroids – protoplanetary disks – radiative transfer – shock waves

Online-only material: animation, color figures

1. INTRODUCTION

Chondrules are submillimeter to millimeter-sized, mostly Fe–Mg silicate spherules found within chondritic meteorites. Chondrule precursors were heated to high temperatures and melted, and then slowly cooled and crystallized to form chondrules, while they were independent, free-floating objects in the early solar nebula. A wealth of elemental and isotopic compositional measurements, as well as mineralogical and petrological information, potentially place important constraints on the melting and cooling of chondrules. The physical conditions and processes acting in the early solar nebula could be deciphered if the chondrule formation mechanism could be understood.

Various chondrule formation models have been proposed. These are assessed against their ability to match the following meteoritic constraints: (1) models must explain why most chondrules appear to have formed only millions of years after the oldest solids formed in the solar nebula (calcium-rich, aluminum-rich inclusions, otherwise known as CAIs). Radiometric (Al–Mg and Pb–Pb) dating shows that nearly all extant chondrules formed $\approx$1.5–4 Myr after CAIs, with the majority forming 2–3 Myr after CAIs (Kurahashi et al. 2008; Villeneuve et al. 2009). (2) Models must explain the high number density of chondrules in the formation region. About 5% of chondrules are compound chondrules, chondrules that fused together while still partially molten (Gooding & Keil 1981; Ciesla et al. 2004a). Based on this frequency and an assumed relative velocity 100 cm s^{-1}, a number density of chondrules $\sim$1–10 m^{-3} has been inferred (Gooding & Keil 1981; Ciesla et al. 2004a). Cuzzi & Alexander (2006) also require a density $>$10 m^{-3} so that the partial pressure of volatiles following

chondrule melting remains high enough to suppress substantial loss of further volatiles. This density is significantly higher than the average density of chondrules in the solar nebula. Based on a silicate-to-gas mass fraction 0.5% (Lodders 2003) and the observation that chondrules comprise 75% of the mass of an ordinary chondrite (e.g., Grossman 1988), we expect the chondrules-to-gas ratio to be 0.375% (although this value may be lower if a large percentage of the available solids are locked up in planetary embryos). Assuming a chondrule mass $m_c = 3.7 \times 10^{-4}$ g, consistent with a chondrule of radius 300 μm and internal density 3.3 g cm^{-3}, and a nebula gas density 1×10^{-9} g cm^{-3} (Desch 2007), we would expect a chondrule number density 0.01 $\mathcal{C}$ m^{-3}, where the chondrules-to-gas mass ratio is defined as $3.75 \times 10^{-3} \mathcal{C}$, with $\mathcal{C}$ representing an additional concentration factor. Here, the chondrule precursor radius of 300 μm is chosen to be consistent with chondrules found in most chondrites. It is reasonable, however, to assume that there was a size distribution between matrix-sized grains and large chondrule precursors in the solar nebula prior to a chondrule-forming event. Morris & Desch (2012) find that cooling rates are increased slightly for simple size distributions, but not enough to affect the general results of the shock model. We therefore consider only a single size for simplicity. In the chondrule-forming region, chondrules appear to have been concentrated by large factors, up to 100 times their background density (for a relative velocity of 100 cm s^{-1}). (3) Models must allow for simultaneous chondrule formation over large regions ($>$10^3 km in size) to limit diffusion of volatiles away from chondrules, in order to keep the partial pressures of the volatiles high enough to suppress isotopic fractionation of these volatiles (Cuzzi & Alexander 2006). Likewise, the

existence of compound chondrules argues for regions larger than the mean free path of a chondrule through a cloud of chondrules, which is 100–1000 km for the densities quoted above. (4) Models must explain the relatively slow cooling of chondrules over hours. Comparison of chondrule petrologic textures with experimental analogs show that the 80% of chondrules in ordinary chondrites that have porphyritic textures (Gooding & Keil 1981) cooled from their peak temperatures at rates ~ 10–10^3 K hr^{-1} and crystallized in a matter of hours (Desch & Connolly 2002; Hewins et al. 2005; Connolly et al. 2006; Lauretta et al. 2006). (5) The partial pressure of Na may have been considerably higher than is easily explained by volatile loss from chondrules. Alexander et al. (2008) recently reported high mass fractions ≈ 0.010–0.015 wt% of Na_2O in the cores of olivine phenocrysts of Semarkona chondrules, indicating that the olivine melt contained substantial Na. The implied partial pressures of Na vapor in the chondrule-forming region are $\sim 10^{-5}$ bar. If this vapor is supplied by the chondrules themselves, chondrule concentrations $\mathcal{C} > 10^5$ would be required. Such a high chondrule concentration would have significant and even incredible physical consequences, but it has been difficult to explain the high Na concentrations in the chondrule olivine by any other method (Alexander et al. 2008). Many additional constraints on chondrule formation exist as well (see Desch et al. 2012). The model that appears most consistent with the constraints on chondrule formation is the nebular shock model, in which chondrules are melted by passage through shock waves in the solar nebula gas (Desch et al. 2005, 2010, 2012). Of the sources of shocks considered to date, two were found to be most plausible by Desch et al. (2005): large-scale shocks driven by gravitational instabilities (e.g., Boss & Durisen 2005; Boley & Durisen 2008) and bow shocks driven by planetesimals on eccentric orbits (e.g., Hood 1998; Ciesla et al. 2004b; Hood et al. 2009; Hood & Weidenschilling 2011).

A planetesimal or other body on an eccentric orbit will inevitably drive a bow shock in front of it because its orbital velocity necessarily differs from that of the gas, which remains on circular orbits with nearly the Keplerian velocity v_K. A body with eccentricity e will have a purely azimuthal velocity at aphelion or perihelion, but one that differs from the local Keplerian velocity by an amount $\sim e v_K / 2$. At other locations in its orbit the protoplanet also has a radial velocity. If the body's orbit is inclined, this also enhances the relative velocity. The combined effect is that the body's velocity relative to the gas can remain a substantial fraction of the Keplerian velocity ($v_K \sim 20$ km s^{-1} at 2 AU) over its entire orbit. As one plausible example, which we discuss further in Section 6.1, we show in Figure 1 the velocity difference V_s between the gas and solid body on an eccentric orbit with semimajor axis $a = 1.25$ AU, eccentricity $e = 0.2$, and inclination $i = 15°$. The relative velocity is seen to vary over the orbit but it remains >3 km s^{-1} at all times. As the typical sound speed in the gas is <1 km s^{-1}, a bow shock is the inevitable result of an eccentric planetary body. The authors listed above (Hood 1998; Ciesla et al. 2004b; Hood et al. 2009; Hood & Weidenschilling 2011) have argued that planetesimals, bodies up to several $\times 10^2$ km in radius, on eccentric orbits, would be common enough to drive sufficient shocks to melt the observed mass of chondrules, which is 2×10^{-4} $M_\oplus$ (Grossman 1988).

Despite their presumed ubiquity, planetesimal bow shocks have not been favored as the chondrule-forming mechanism. Because chondrules are associated with asteroids and formation in the asteroid belt, only planetesimals $\lesssim 10^3$ km in diameter
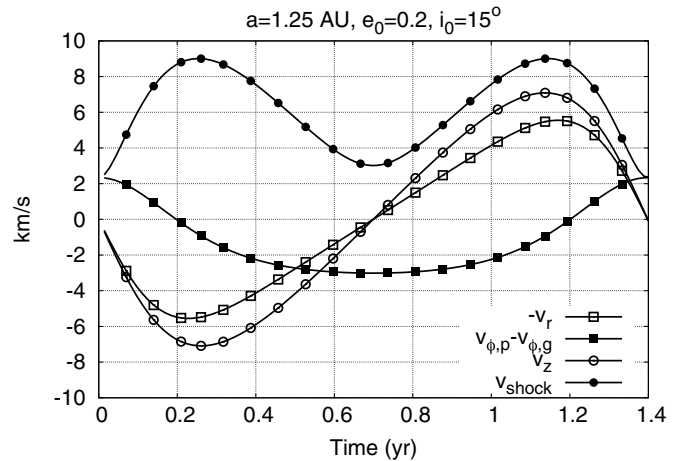
Figure 1. Velocity difference V_s between nebular gas (on a circular Keplerian orbit) and a planetary embryo on an eccentric orbit with semimajor axis $a = 1.25$ AU, eccentricity $e = 0.2$, and inclination $i = 15°$. The radial, azimuthal, and vertical components, and the total velocity difference V_s (equal to the speed of the bow shock) are shown as functions of time over the orbit, where $t = 0$ signifies perihelion passage. In this example, the planet passes through the ascending node at $t \approx 1.1$ years. V_s is supersonic and bow shocks are driven throughout the orbit.

have been considered so far. For such bodies, the size of the heated region, which is necessarily comparable to the size of the planetesimal itself, is probably too small to satisfy the above constraints on the chondrule-forming region. More importantly, the small size of the heated region means chondrules are never far from cold, unshocked gas to which they can radiate and cool. The optically thin geometry is expected to lead to very fast cooling rates, and matching the cooling rates necessary to reproduce the dominant porphyritic texture in particular, $\lesssim 10^3$ K hr^{-1}, requires physical conditions that appear extreme (e.g., Ciesla et al. 2004b; Morris et al. 2010a, 2010b). Intuitively, suppression of the radiation that cools the chondrules requires the optical depth τ between the chondrule-forming region and the unshocked gas to be $\gtrsim 1$. In their treatment of the problem, Morris et al. (2010a, 2010b) found that optical depths $\tau \gtrsim 0.1$ led to cooling rates $\sim 10^3$ K hr^{-1}, just barely consistent with the constraints. Our treatment of chondrule cooling here (see Section 4) suggests slightly slower cooling, but the cooling rates ~ 100 K hr^{-1} consistent with porphyritic textures require optical depths $\tau \sim 0.1$. The optical depth is a function of the opacity and the size of the region. Dust grains that might otherwise increase the opacity are found to vaporize in shocks strong enough to melt chondrules (Morris & Desch 2010). The opacity of chondrules themselves, at their background levels, does not yield $\tau > 0.1$ unless the size of the region is $l \gg 3 \times 10^4$ km. Even if chondrules are concentrated by the considerable factor of 100 times their background level, so that $n_c = 1$ m^{-3}, planetesimals at least several hundred kilometers in radius are required to yield marginally consistent cooling rates (Ciesla et al. 2004b; Morris et al. 2010a, 2010b). To the extent that mass is locked up in large planetary bodies rather than dust and chondrule-sized objects, even higher concentrations of chondrules above background levels are required.

Another difficulty of the planetesimal bow shock model, one that has not been discussed previously, is that due to the small size of the planetesimal, chondrule precursors passing close enough to the body to be melted as chondrules are likely to be

accreted by the planetesimal. Unlike the gas, whose velocity is immediately altered at the shock front to flow around the body, chondrules have sufficient inertia that they retain their pre-shock velocity until they have collided with their own mass of gas. Chondrules can be deflected around the body driving the bow shock only by moving a minimum length through the gas past the shock front. For typical parameters this length is ≈300 km. The stand-off distance between the bow shock and a 500 km radius planetesimal driving it is typically ≲100 km (see Section 2), meaning that accretion onto the planetesimal is probable. This is problematic because chondrules are expected to mix with cold nebular components before accretion, and a given chondrite will contain chondrules with a wide variety of ages.

Chondrules melted in bow shocks around bodies *larger* than planetesimals may conform better to the constraints on chondrule cooling rates and the size of the chondrule-forming region. The terrestrial planets have long been recognized to have formed from planetary embryos, bodies >1000 km in diameter or even much larger, and it has been recognized that these embryos could have formed in a few Myr or less (Wetherill & Stewart 1993; Weidenschilling et al. 1997). Mars itself is considered a starved planetary embryo (Chambers & Wetherill 1998), which allows the timing of embryo formation to be fixed. Previous Hf–W isotopic analyses had suggested Mars had differentiated within 10 Myr of CAI formation (Nimmo & Kleine 2007). More recently, the analysis of Hf and W, in conjunction with Th, by Dauphas & Pourmand (2011) suggests that Mars accreted 50% of its mass (and 80% of its radius) within 2 Myr of CAIs. Formation of the terrestrial planets requires dozens of such embryos. The timing of Mars's formation establishes that the solar nebula contained not just planetesimals, but *protoplanets*, during the epoch of chondrule formation.

Moreover, some of these planetary embryos quite plausibly found themselves on eccentric orbits at least some of the time. Mutual scattering events are common in *N*-body simulations (Chambers 2001; Raymond et al. 2006). One recent model for the origin of Mars in particular suggests that it suffered close encounters with other bodies in an annulus interior to 1 AU, and was scattered into an inclined, eccentric orbit with aphelion at 1.5 AU (Hansen 2009). Alternatively, Walsh et al. (2011) have simulated the early migration of Jupiter and have shown that it leads to a truncated inner disk (consistent with the Hansen 2009 model) and an excess of dynamically excited planetary embryos (at least 5 in number) at 1.0 AU, from which they propose Mars formed. The true extent to which embryos were scattered is not well known, but is a common feature of planet formation models.

The recent confirmation by Dauphas & Pourmand (2011) that large planetary embryos did exist at the time of chondrule formation, the expectation that such planetary embryos may be scattered onto eccentric orbits, and the larger size of the chondrule-forming region around planetary embryos strongly motivate us to consider chondrule formation in bow shocks around planetary embryos several 1000 km in radius. Despite the obvious similarities to chondrule formation in planetesimal bow shocks, chondrule formation in planetary embryo bow shocks differs in several significant ways. First, as the planetary radius and size of the chondrule-forming region increase above a threshold of about 1000 km (for the embryo radius), the region of heated chondrules becomes optically thick, fundamentally altering the chondrule cooling rates. Second, chondrules flowing around bodies larger than about 1000 km in radius can dynamically recouple with the gas and avoid hitting the embryo's

surface. Chondrules in planetesimal bow shocks, if their impact parameters are less than the planetesimal radius, are likely to be accreted by the planetesimal. A third fundamental difference is that planetary embryos larger than about 1000 km in radius are able to accrete a primary atmosphere from the nebula and retain secondary outgassed atmospheres. The escape velocity from a body with radius R_p and Mars-like density ($\rho = 3.94$ g cm^{-3}) is $1.5 (R_p/1000$ km$)^{1/2}$ km s^{-1}, compared to a typical sound speed 0.7 km s^{-1} (at 150 K). The atmosphere retained by the larger planetary embryo will affect the trajectories of gas and chondrules flowing past it, and will also alter the chemistry of the chondrule formation environment. We are motivated to study chondrule formation in planetary embryo bow shocks because of these fundamental differences.

Here we present new calculations of the melting of chondrules in bow shocks around large protoplanets on eccentric orbits. We show that for reasonable parameters, chondrule formation in planetary embryo bow shocks is consistent with the major constraints listed above. We show that for the largest eccentricities and inclinations we consider plausible the shocks speeds of 6–8 km s^{-1} needed for chondrule formation (Morris et al. 2010a, 2010b; Section 4) are sustained for much of the protoplanet's orbit. For the first time, we follow the trajectories of chondrules formed in bow shocks and demonstrate that they are not accreted by the protoplanet, whereas chondrules formed in bow shocks around planetesimals *are* accreted. Based on the spatial distribution of chondrules, we calculate the optical depths and calculate chondrule cooling rates. We show that the large scale of planetary embryo bow shocks yields chondrule cooling rates consistent with meteoritic constraints. We show that chondrules formed in planetary embryo bow shocks do pass through what is essentially the planet's upper atmosphere, and therefore may be exposed to high vapor pressures of species outgassed from the protoplanet's magma ocean, including H_2O and Na vapor. We compute the rate at which a protoplanet's eccentricity and inclination are damped, and show that the protoplanet's orbit remains eccentric and can drive shocks for $\sim 10^5$ yr. We find that a single scattered planetary embryo can process up to 10^{24} g of chondrules.

2. HYDRODYNAMICS OF PLANETARY EMBRYO BOW SHOCKS

We have numerically investigated the hydrodynamics of a bow shock around a planetary embryo using the adaptive-mesh, Eulerian hydrodynamics code, FLASH (Fryxell et al. 2000). We consider a stationary protoplanet on a cylindrical (axisymmetric) two-dimensional (2D) grid. We simulate the relative motion of the protoplanet through the gas by imposing a supersonic inflow of gas along the symmetry axis, originating at the $-z$ boundary. Our assumed boundary conditions allow for inflow on the $-z$ boundary, reflection on the symmetry axis, and diode (zero-gradient) boundary conditions on the other boundaries. We consider two physical cases: that of a planetesimal and one of a planetary embryo.

In the first case of a planetesimal, we consider a body with mass $M_p = 2 \times 10^{24}$ g, a radius of $R_p = 500$ km, yielding a density of 3.80 g cm^{-3} (similar to Mars's density). The computational domain has a radius of 16,000 km and a vertical extent of 32,000 km. The simulation is run with seven levels of refinement, resulting in our best grid resolution of 32 km $= X_{size}/[N_{X_{block}} \cdot 2^{(\text{levels of refinement}-1)}]$, where $N_{X_{block}} = 8$. In the second case of a planetary embryo, motivated by the results

of Dauphas & Pourmand (2011), we initialize our simulations with a protoplanet of mass $M_p = 3.20 \times 10^{26}$ g (half of Mars's mass) and a radius $R_p = 2720$ km (80% of Mars's radius), with density 3.80 g cm^{-3}.

Once again, the computational domain has a radius of 16,000 km and a vertical extent of 32,000 km, and the simulation is run with eight levels of refinement. In both cases the body is embedded in a non-radiating H$_2$/He gas with uniform initial density $\rho_0 = 1.0 \times 10^{-9}$ g cm^{-3}, pressure $P_0 = 5.3 \times 10^{-6}$ atm, temperature $T_0 = 150$ K, and assumed adiabatic index $\gamma = 7/5$, appropriate for the solar nebula at around 2 AU (Desch 2007). The gravitational pull of the protoplanet was simulated using a point-mass gravity module.

Before we initialize the inflow, we allow the planetary embryo to acquire a primary atmosphere of H$_2$ and He. It is straightforward to show that accretion of adiabatic gas will lead to a spherically symmetric profile

$$\rho(r) = \rho_0 \left[1 + \frac{r_g}{r}\right]^{1/(\gamma-1)}, \qquad (1)$$

where r is the distance from the protoplanet center and $r_g = (\gamma - 1)(GM_p\rho_0/P_0)/\gamma$ is akin to a scale height. For the case of the planetesimal, $r_g \approx 71$ km, and the atmosphere that develops is very thin and hardly resolveable by our best grid resolution of 32 km. Physically it behaves as part of the planetesimal surface in our runs. For the case of the planetary embryo, $r_g \approx 11,500$ km. At the protoplanet *surface* the density is expected to reach 6.2×10^{-8} g cm^{-3}, the pressure to reach 1.74×10^{-3} bar, and the temperature to reach 780 K, values that are 62.5, 330.0, and 5.2 times their background values, respectively. The effective scale height near the protoplanet surface is ≈ 1000 km, and is easily resolved by our best resolution of 32 km. The primary atmosphere acquired by the planetary embryo in our simulations matched this solution within a few percent. The mass of the atmosphere inside 1000 km of the protoplanet surface is very nearly 3×10^{18} g, also in accord with analytical estimates. We do not directly simulate the effects of a secondary atmosphere of species outgassed from the protoplanet's magma ocean, which would be orders of magnitude denser, but we expect it would behave very similarly dynamically.

We begin our simulation of the bow shock with the protoplanet and primary atmosphere, and introduce gas streaming up from the lower z boundary with density $\rho_0 = 1 \times 10^{-9}$ g cm^{-3} and upward velocity $V_s = 8$ km s^{-1}. We chose this density to represent conditions of the chondrule-forming region, presumed to be at 2–3 AU (but, see Section 6). However, disk models differ on gas densities in the protoplanetary disk. For example, the density $\rho_0 = 1 \times 10^{-9}$ g cm^{-3} is achieved in a minimum-mass solar nebula model (Hayashi 1981) at 1.25 AU (depending on the scale height) or at several (up to 5) AU in more massive disk models (Desch 2007). We chose the relative velocity of 8 km s^{-1} based on the results of Morris & Desch (2010), who showed that this speed was necessary to achieve chondrule melting. Such a large relative velocity may appear to be extreme, but such values are expected to be met episodically throughout planet formation, even though the typical relative velocity is expected to be much lower. A velocity difference of 8 km s^{-1} between the body and the gas can occur for a range of eccentricities and inclinations, which will be explored in more detail in Section 6. Here, consider the example of a body on an orbit with a semimajor axis $a = 1.25$ AU and $e = 0.29$. This body will produce an ~ 8 km s^{-1} bow shock at quadrature ($a \sim 1.1$ AU),
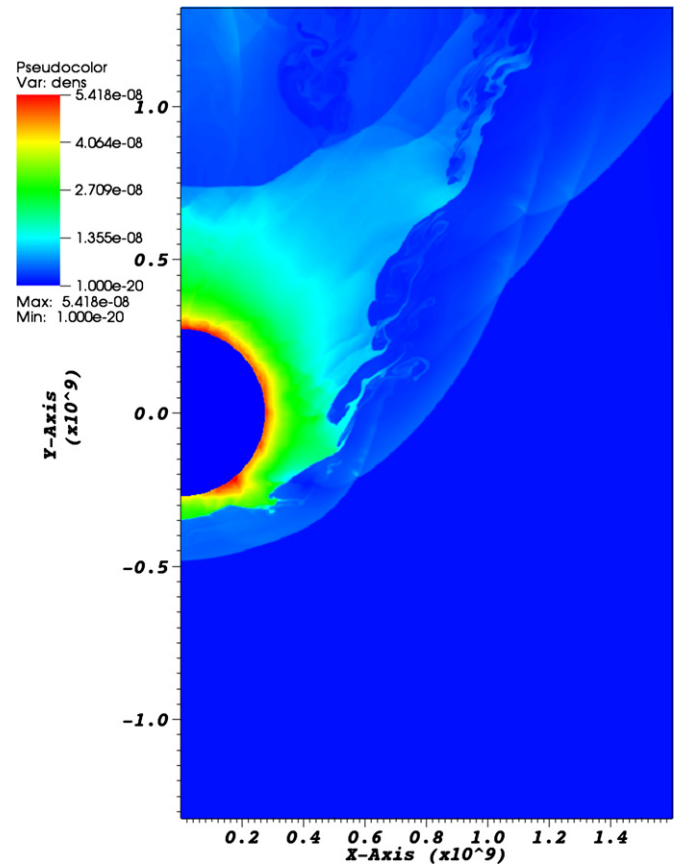

Figure 2. Evolution of a bow shock around a planetary embryo with radius 2720 km (i.e., half a Mars mass) on an inclined and eccentric orbit.

(An animation and a color version of this figure are available in the online journal.)

which is a plausible site for the formation of some chondrules. Compared with the total population of embryos, such high relative velocities may be rare, but when they do occur, they can be very significant, as we will show.

In both the planetesimal and planetary embryo cases, the evolution of the gas is marked by a reverse shock bouncing off the body surface and multiple shocks reflecting off each other at the symmetry axis. Within a few crossing times (i.e., a few $\times 10^3$ s) for the planetesimal case, and a few $\times \sim 10^4$ s for the planetary embryo case), a quasi steady-state bow shock structure is reached. An animation showing the case for the protoplanet is shown in Figure 2. Contour plots of gas densities 4×10^4 s after the introduction of supersonic material on the grid is shown in Figure 3. In both panels the gas density is depicted in blue, with the darkest levels referring to densities of 2.5×10^{-10} g cm^{-3} and the brightest levels to 2.5×10^{-8} g cm^{-3}. At the bow shock itself the density increases by a factor of six at the shock front, from 1×10^{-9} g cm^{-3} to 6×10^{-9} g cm^{-3}, as expected for a $\gamma = 7/5$ gas, in a strong shock.

We observed that the bow shock around the planetesimal quickly achieved steady state, but as is evident from Figure 3 (right), steady state is not formally achieved around the protoplanet. This is observed by the varying density in the wake of the protoplanet, and the slightly irregular structure of the bow shock (e.g., the kink at $x = 6000$ km). We attribute this to the boundary layer that exists between the primary atmosphere and the post-shock flow of gas past the protoplanet. Inside this boundary, evident at a distance ≈ 1000 km from the protoplanet
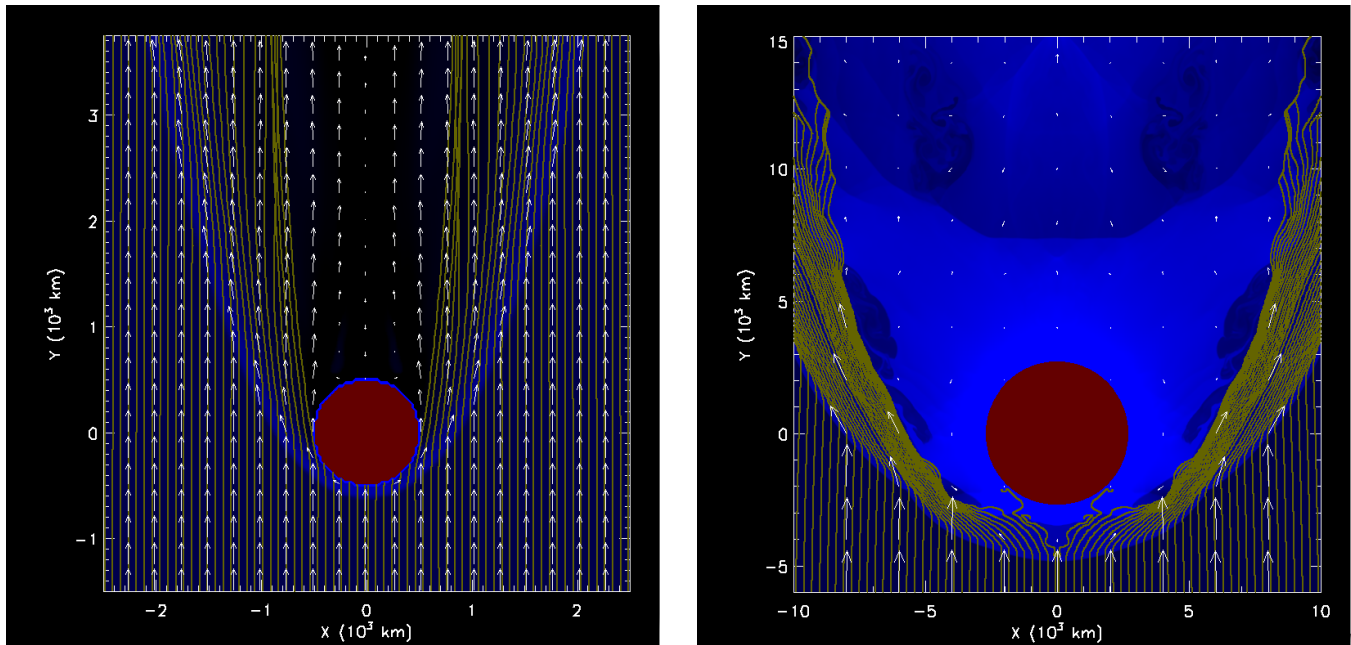
Figure 3. Left: gas density (blue contours) and velocities (white arrows) and trajectories of chondrule precursors/chondrules (gold streamlines) in the vicinity of the bow shock surrounding a 500 km radius planetesimal. Velocities are measured in the frame of the planetesimal, moving at $8\,\mathrm{km\,s^{-1}}$ with respect to the local gas. Chondrules with impact parameters $\lesssim 460$ km are accreted. Right: the same plot repeated for a planetary embryo with radius 2720 km (i.e., half a Mars mass). Note the change in scale. In this case, particles with impact parameter $\gtrsim 400$ km are *not* accreted.

(A color version of this figure is available in the online journal.)

surface, the densities are considerably higher ($>10^{-8}\,\mathrm{cm^{-3}}$) than the densities $\approx 6 \times 10^{-9}\,\mathrm{g\,cm^{-3}}$ between this boundary and the bow shock. This boundary is unstable to the Kelvin–Helmholtz (KH) instability, and we observed frequent shedding of vortices and rolls of material at this interface; these rolls are evident in Figure 3 (right) at regular (≈ 2000 km) intervals. Reflections of sound waves off of these rolls are responsible for the irregular structure at the bow shock.

Eventually these KH rolls will strip away the atmosphere surrounding the protoplanet. Numerical simulations of the stripping of gravitationally bound gas by KH rolls at the surfaces of protoplanetary disks by Ouellette et al. (2007) suggest that the efficiency of stripping is about 1%, meaning that the mass of gas that is stripped is about 1% of the mass of the impacting gas. Based on the inflow of gas $\rho_0 \pi R_p^2 V_s$, we estimate a stripping rate $2 \times 10^{12}\,\mathrm{g\,s^{-1}}$. This suggests that loss of the primary atmosphere would take $>10^6$ s, hundreds of times longer than the duration of our simulation. We were able to quantify this stripping rate via a "dye" calculation in which we kept track separately of material accreted before the supersonic flow of gas on the grid. We found that after an initial loss of gas, the primary atmosphere was being lost on timescales $\sim 10^5$ s, suggesting a stripping rate $>10^{13}\,\mathrm{g\,s^{-1}}$. The existence of this interface between an atmosphere and the post-bow shock flow is a fundamental difference between the planetesimal and protoplanet cases.

3. CHONDRULE TRAJECTORIES IN PLANETARY EMBRYO BOW SHOCKS

Having established the dynamics of the gas and the structure of the bow shock surrounding the planetary embryo, we now turn our attention to the trajectories of chondrules and their precursors in the flow. In general, the particles are dynamically coupled to the gas, except in the vicinity of the bow shock,

when the gas suddenly changes velocity over a few molecular mean free paths (i.e., over a few meters). Particles will dynamically recouple with the gas on a timescale comparable to the aerodynamic stopping time,

$$t_{\mathrm{stop}} = \frac{\rho_s a_c}{\rho_g c_s}, \qquad (2)$$

where $\rho_s \approx 3\,\mathrm{g\,cm^{-3}}$ is the particle internal density, $a_c \approx 300\,\mu\mathrm{m}$ is its radius, ρ_g is the post-shock gas density, and c_s is the post-shock gas sound speed. For $\rho_g = 6 \times 10^{-9}\,\mathrm{g\,cm^{-3}}$ and $T_g \approx 2500$ K, the stopping time is 50 s. If the planetary body is traveling through the gas at a speed $V_s = 8\,\mathrm{km\,s^{-1}}$, particles will move past the shock front several hundred km before they dynamically couple to the gas. Based on the numerical simulations above, this length scale is less than or comparable to the distance between the shock front and the planetary bodies themselves. The expectation is that particles passing through a bow shock will be accreted onto a planetesimal and will flow around a planetary embryo, although clearly a careful calculation of the trajectories is required to determine their fate.

We are also motivated to calculate the trajectories of particles carefully to determine if they will melt and cool in a manner consistent with chondrules. The maximum heating of the chondrules is set by their velocity relative to the gas after passing through the shock front, which sets their degree of melting. Their cooling after melting is set by the optical depth between the particles and the unshocked gas, which in turn is set by the geometry and spatial distribution of the particles. These must be calculated numerically.

We have computed the trajectories of particles by integrating the particles' motions through the gas, assuming the gas flow around the planetary body is in a steady state. We assume the particles are tracers only, with no dynamical effect on the gas. Particles are accelerated by the gravity of the planetary embryo

(with mass M_p) and by the drag force due to gas of density ρ_g:

$$m_c \frac{dV_c}{dt} = -\frac{GM_p m_c}{r^3} \, \boldsymbol{r} - \pi a_c^2$$
$$\times \left(\frac{C_D}{2}\right) \rho_g \, |V_c - V_g| \, (V_c - V_g), \qquad (3)$$

where $\boldsymbol{r}$ is the position vector of the chondrule (with respect to the planet center), and V_c and V_g are the chondrule and gas velocities. Particles are in the Epstein limit (much smaller than the mean free paths of gas molecules), and the drag force is given by

$$C_D = \frac{2}{3s}\left(\frac{\pi T_c}{T_g}\right)^{1/2} + \frac{2s^2+1}{\pi^{1/2}s^3}\exp(-s^2) + \frac{4s^4+4s^2-1}{2s^4}\,\mathrm{erf}(s),$$
$$(4)$$

where we will assume the particle temperature T_c locally equals the gas temperature T_g, and where

$$s = \frac{|V_c - V_g|}{(2kT_g/\bar{m})^{1/2}}, \qquad (5)$$

where $\bar{m} = 2.33 m_H$ is the mean molecular weight of the gas and k is Boltzmann's constant (Probstein 1968). Gas velocities V_g, temperatures T_g, and densities ρ_g are found from the output of the hydrodynamic simulations, using bilinear interpolation on a grid with spatial resolution of 32 km. Particle velocities are integrated using a simple explicit scheme that is first order in time, with time steps of 0.05 s. Particles move no more than 0.4 km during each time step, which is significantly smaller than the spatial resolution of the hydrodynamics simulations.

The trajectories of chondrules around both the planetesimal and the planetary embryo are depicted in Figure 3. These are seen to be significantly affected by the size of the region between the shock front and the body. At the shock front the gas undergoes a nearly instantaneous shift in velocity. Chondrules regain dynamical equilibrium with the gas only after they move through the gas by a stopping length $V_{rel}t_{stop}$, where t_{stop} is the stopping time (Equation (2)) and V_{rel} is the velocity of a chondrule with respect to the gas. This quantity depends only on the gas density ρ_g, not the radius of the planetary body. For both the planetesimal and planetary embryo cases, the stopping time $t_{stop} \approx 50$ s (assuming a gas density $\rho_g = 1 \times 10^{-9}$ cm^{-3}), over which time the chondrules slow from a velocity (relative to the planet) of 8 km s^{-1} to about 2 km s^{-1}. Assuming an average velocity $\approx$5 km s^{-1}, chondrules will typically move about 250 km past the shock front. This stopping length is to be compared to the size of the post-shock region, specifically the standoff distance between the shock front and the planetary body itself. For the $R_p = 500$ km planetesimal case, this standoff distance between the shock front and the planetesimal is $\approx$110 km $\approx 0.2\,R_p$. It is therefore not surprising that all chondrules with impact parameter $b < 460$ km are accreted onto the planetesimal. In contrast, for the $R_p = 2720$ km planetary embryo case, the standoff distance to the planet is $\approx$2000 km $\approx 0.8\,R_p$, or $\approx$1400 km $\approx 0.5\,R_p$ to the atmosphere, much greater than the stopping length. Thus, the vast majority of chondrules dynamically recouple with the gas before hitting the planet. Only those chondrules with $b \lesssim 400$ km might be accreted, and chondrules that escape accretion flow around the body. Along the way, their trajectories are affected by the KH instabilities

between the shocked gas and the primary atmosphere. This makes it difficult to predict their *exact* trajectories, but it is clear that they will escape accretion onto the body.

Moving forward it is important to distinguish between particles that pass through the shock front more directly and are melted as chondrules, and those particles that pass through the shock front far from the body and are not melted as chondrules. Only particles that pass through the shock front with sufficient velocity V_{rel} relative to the gas will melt as chondrules. The heating rate of chondrules after they pass through the shock front scales as V_{rel}^3 (up to the liquidus temperature). As we discuss in Section 4, a shock speed of 6 km s^{-1} is required to ensure melting of chondrules, which is equivalent to $V_{rel} \gtrsim 5$ km s^{-1}. The relative velocity between chondrules and gas is a function of the impact parameter b, and is easily calculated for the case $b = 0$ km (chondrules and gas impact the body directly). Just past the shock front, chondrules retain their velocity but gas is immediately slowed by a factor of $(\gamma + 1)/(\gamma - 1) \approx 6$. The velocity difference between gas and chondrules is thus $\approx$(5/6)(8 km s^{-1}) $\approx$6.7 km s^{-1}. As the impact parameter b is increased, this relative velocity decreases. This is because only the component of the velocity normal to the shock front is reduced, whereas the tangential component of velocity is conserved. As b increases and the shock becomes increasingly oblique, the relative velocity is decreased, and therefore the chondrule heating rate is decreased. We therefore anticipate a maximum impact parameter for precursors to be melted as chondrules.

This variation of relative velocity with impact parameter is indeed seen in our numerical simulations, as illustrated in Figure 4 (left; planetesimal case) and Figure 4 (right; planetary embryo case). In both cases, the maximum relative velocity at $b = 0$ km approaches $\approx$6.7 km s^{-1}, and decreases with increasing impact parameter. In the $R_p = 500$ km case, the relative velocity drops below the critical threshold for melting, 5 km s^{-1}, for impact parameters $\gtrsim$400 km. For the $R_p = 2720$ km planetary case, on the other hand, particles experience $V_{rel} > 5$ km s^{-1} for impact parameters as high as $b \approx 4300$ km. If the planetary embryo had even higher speed with respect to the gas, this maximum impact parameter would be expanded. Because of the slightly irregular shape of the shock front, some regions are not as oblique as others. In the snapshot of Figure 3 (right), for example, particles with $b \approx 6000$ km encounter the shock more directly and may experience thermal histories consistent with chondrules. Note that even particles with $b = 10,000$ km will be significantly heated (by a shock with speed 2.5 km s^{-1}), but will not be melted as chondrules. Comparing the cross-sections, the vast majority (>80%) of particles encountered by the bow shock will be heated, but not melted.

There is generally a maximum impact parameter for which particles are melted as chondrules, but a minimum impact parameter for which particles escape accretion. For a planetesimal with radius $R_p = 500$ km, only particles with $b < 400$ km are heated strongly enough to melt as chondrules. However, only particles with $b > 460$ km escape accretion onto the planetesimal. From this we see that *all* particles melted as chondrules in a planetesimal bow shock are accreted onto the planetesimal. For a planetary embryo with a radius of $R_p = 2720$ km, on the other hand, all particles with $b < 4300$ km (possibly up to 6000 km) are melted as chondrules, whereas only particles with $b < 400$ km are possibly (but not necessarily) accreted. More than 99% of all particles melted as chondrules in a planetary embryo bow shock escape accretion by the body. Larger bodies
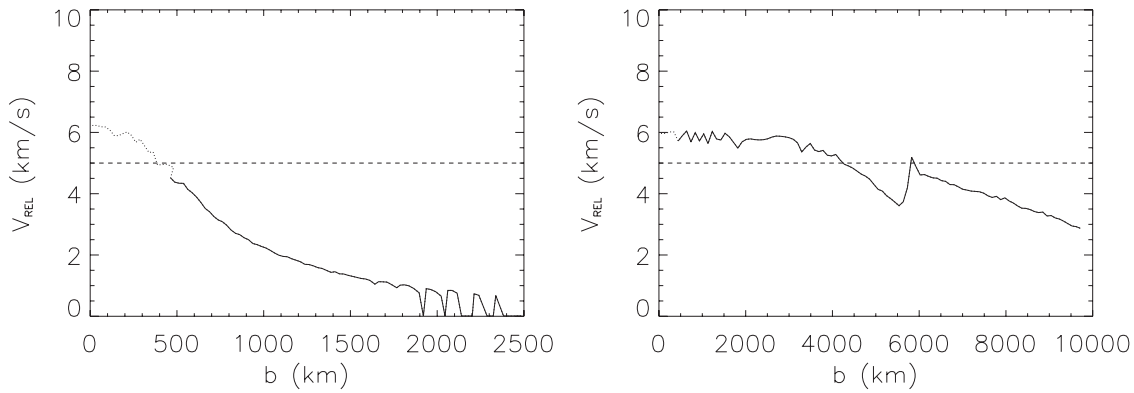
Figure 4. Left: maximum relative velocity between chondrules and gas, achieved just after passing through the bow shock, as a function of the impact parameter b, for the $R_p = 500$ km case. Values of b that lead to the chondrules being accreted are plotted with a dotted line instead of a solid line. The minimum relative velocity needed for chondrules to melt (= 5 km s^{-1}) is shown. Right: same but for the $R_p = 2720$ km case. Only particles with $b \lesssim 400$ km might be accreted.

will present a larger shock front to incoming particles, increasing the impact parameter out to which chondrules form, and will produce shocks that stand off farther from the body, decreasing the fraction of particles accreted.

One important caveat to the results stated above is that the chondrule trajectories were calculated under the assumption that the gas flow was in steady state. This assumption is valid for gas as it flows to the shock, and even in the immediate post-shock region, but is manifestly not valid at the boundary where the post-shock gas flows past the planetary atmosphere, since this boundary is strongly affected by KH rolls. Figure 3 (right) makes clear that where chondrules intercept a KH roll (e.g., at impact parameters 2000 km and 5000 km), the gas flow drives chondrules out of the KH roll. Likewise, at impact parameter ≈4000 km, characterized by the absence of KH rolls, the gas is flowing from the shock front inward, driving chondrules into the void. Thus, there is a tendency for chondrules to "skim" the boundary surface between the atmosphere and the post-shock gas, although it is difficult to confirm this tendency under the assumption of a steady-state flow. Chondrules in the vicinity of the flow-atmosphere boundary have a range of velocities ≈1.8–5.6 km s^{-1} (see below), while the KH rolls themselves have velocities (pattern speeds) on the order of 3.5 km s^{-1}, so that chondrules will probably move in and out of KH rolls, but not at the rates they do so in this calculation, in which the gas flow is kept in steady state.

The trajectories of chondrules determine their density in the chondrule-forming region. In what follows, we specifically focus on particles that achieved temperatures high enough to melt as chondrules. To be specific, we consider the particles processed by the planetary embryo bow shock in Figure 3 (right) which will pass through a slice with $Y = +3000$ km near the shock front, with $X \approx 7000$–10,000 km. Considering just the subset of those particles that melted as chondrules, they have impact parameters $b = 400$–4300 km, and pass through $X = 7180$–8060 km. Particles with the lower end of impact parameter ($b = 400$ km) move most slowly, at speeds ≈1.8 km s^{-1}, and take 2–4 hr to reach this region. Chondrules with the higher impact parameter ($b = 4300$ km) tend to have speeds ≈5.6 km s^{-1} and take just under 1 hr to reach this region. On average, chondrules' velocities are reduced from their pre-shock values (8 km s^{-1}) by factors ≈2.3, implying that chondrule densities will increase by a factor of 2.3 as they slow. In addition, the chondrules are also seen to be geometrically concentrated as they are funneled into a smaller

conical volume past the bow shock. This increases their density by a factor of $(4300^2 - 400^2)/(8060^2 - 7180^2) = 1.37$. Combined, the chondrule density is raised above the background value by a factor of 3.2. A similar calculation for those particles with impact parameters 4300 km < b < 10,000 km shows the density of these particles is increased by a similar factor. These particles will not have achieved the same peak temperatures as those particles with smaller impact parameters, but they will be almost as hot. For example, if particles with $b = 0$ km achieved peak temperatures of 2000 K, and peak temperature scales as $V_{rel}^{3/4}$, then Figure 3 (right) suggests that particles with $b = 8000$ km will have peak temperatures ≈1400 K.

The chondrule densities derived above bear on the frequency of compound chondrules. The mean free path of a chondrule in a sea of chondrules is $l_{mfp} = (n_c\,4\pi a_c^2)^{-1}$. For $a_c = 300\,\mu$m and assuming a compression of a factor of 3.2 in the post-shock region, we find $l_{mfp} \approx 2.7 \times 10^4\,\mathcal{C}^{-1}$ km. For $\mathcal{C} = 10$, the mean free path is 2700 km (about the radius of the planet). Within the part of the flow containing chondrules, their velocities range between 1.8 and 5.6 km s^{-1} over a distance 800 km, shorter than the mean free path. Chondrules therefore will collide with other chondrules at relative velocities ΔV up to and above that needed to shatter chondrules, which has been estimated to lie in the range 1 m s^{-1} (Kring 1991) to 100 m s^{-1} (Gooding & Keil 1981). We assume a median threshold for shattering of 10 m s^{-1}, assert that collisions with chondrules up to (and beyond) this speed will occur, and that these will dominate the production of compound chondrules. The compound chondrule frequency f we predict is

$$f = (\Delta V)t_{plast}l_{mfp}^{-1} = 0.04 \left(\frac{\Delta V}{10\,\text{m s}^{-1}}\right)\left(\frac{t_{plast}}{10^4\,\text{s}}\right)\left(\frac{\mathcal{C}}{10}\right),$$
(6)

where t_{plast} is the time for which chondrules remain plastic enough to stick after a collision. The observed frequency of compound chondrules is reproduced in a planetary embryo bow shock assuming chondrules are concentrated by factors $\mathcal{C} \approx 10$, although the exact percentage will depend on the maximum speed at which chondrules can collide and stick without shattering.

Finally, the density of chondrules in the post-shock region will also bear on the optical depths between chondrules and the cool, unshocked gas, which we estimate as follows. The optical depth is $\tau = n_c\,(\epsilon\pi a_c^2)\,l$, where l is the distance between the locations of chondrules and the bow shock, and $\epsilon\pi a_c^2$ is the

wavelength-integrated absorption cross-section, with $\epsilon \approx 0.8$ in the near-infrared (Li & Greenberg 1997). Dust evaporates at the shock front, so the opacity is due solely to chondrules (Morris & Desch 2010). The number density of chondrules in the background nebular gas is

$$n_{c,0} = \frac{(\rho_c/\rho_g)\rho_g}{4\pi\rho_s a_c^3/3} \approx 1 \times 10^{-8}\, \mathcal{C}\, \text{cm}^{-3}, \qquad (7)$$

where we have assumed a chondrule radius $a_c = 300\,\mu m$, an internal density $\rho_s = 3.3\,\text{g cm}^{-3}$, and defined $\mathcal{C} \equiv (\rho_c/\rho_g)/(3.75 \times 10^{-3})$. We estimate l by considering those chondrules (objects with $b < 4300\,\text{km}$) with most probable impact parameter, $b \approx 3000\,\text{km}$. These chondrules pass $Y = +3000\,\text{km}$ at $X \approx 7800\,\text{km}$. The particles with the largest impact parameter to be chondrules ($b = 4300\,\text{km}$) pass through $Y = +3000\,\text{km}$ at $X = 8060\,\text{km}$. Importantly, though, even particles with $b = 8000\,\text{km}$ will achieve near-chondrule-like temperatures of 1400 K, and pass through $Y = +3000\,\text{km}$ at about $X = 9000\,\text{km}$. The unshocked gas lies at $X > 10,000\,\text{km}$ at $Y = +3000\,\text{km}$. Thus, the typical chondrule lies 250 km from the edge of the cloud of particles shocked enough to melt as chondrules, but 2100 km from the bow shock (after correcting for the tilt of shock front). We assume chondrules lie 2200 km from the bow shock and consider chondrules to be concentrated above their background value by a factor of 3.2, to find

$$\tau = 0.16 \left(\frac{\mathcal{C}}{10}\right) \left(\frac{l}{2200\,\text{km}}\right). \qquad (8)$$

The gradual spatial transition from shocked chondrules to unshocked gas makes it difficult to define l more exactly. Nevertheless, this calculation demonstrates that if chondrules are concentrated by factors of about 10, then $\tau \sim 0.16$ for most chondrules melted by planetary embryo bow shocks.

4. THERMAL HISTORIES OF CHONDRULES IN PLANETARY EMBRYO BOW SHOCKS

Having calculated the trajectories of chondrules past the planetary embryo, an important goal is to calculate their thermal histories. These are influenced strongly by the absorption of infrared radiation emitted by nearby chondrules and by the proximity of a cooler region into which the chondrules can radiate (without receiving a return of radiation). In the previously studied cases of large-scale shocks driven by disk-wide gravitational instabilities (e.g., Morris & Desch 2010), the shock front is planar and the geometry is one dimensional (1D). The cooler region into which chondrules radiate is the pre-shock gas (ahead of a radiation front). Chondrule trajectories are parallel to each other and normal to the shock front, and chondrule properties do not vary in the lateral direction. In contrast, following melting by a bow shock around a planetesimal or planetary embryo, the cooler region to which chondrules radiate is in the lateral direction, and the shock clearly has a 2D geometry. The only correct way to calculate chondrule thermal histories is to compute the fully 2D radiation field in cylindrical geometry, but the chondrule trajectories displayed in Figure 3 (right) suggest that a perturbation to the 1D chondrule thermal histories may yield an adequate solution.

First, the particles are seen to flow in a more or less laminar fashion without crossing paths. This suggests that chondrule thermal histories are a function of distance past the shock front, as in the 1D example. Second, chondrules on parallel trajectories

do not differ from each other significantly. As stated above, it takes about 3 hr for chondrules with the lowest initial impact parameter ($b = 400\,\text{km}$), and about 1 hr for chondrules with the highest impact parameter ($b = 4300\,\text{km}$), to reach a certain representative point downstream ($Y = +3000\,\text{km}$). We show below that typical chondrule cooling rates are roughly 60 K hr^{-1}, so that at this location all chondrules are within about 100 K of each other. Compared to the typical chondrule temperature at this location ($\approx 1600\,\text{K}$), this difference is not significant. Third, these properties hold even as the particles move downstream by roughly 20,000 km (not shown in Figure 3 (right)). Further downstream, rarefaction of the shocked gas is presumed to take place. Indeed, some hints of this are seen in the slightly diverging chondrule trajectories in Figure 3 (right), but this does not affect the gross geometry. Certainly the flow remains basically the same for at least the 5 hr it takes for chondrules in our simulations to cool below their solidus temperatures. These facts suggest that a simple alteration to the 1D code of Morris & Desch (2010), to allow for loss of energy by radiation into the unshocked gas, may allow a useful estimate of chondrule thermal histories.

We accommodate for radiative losses in an approximate way using the formulation of Morris et al. (2010a, 2010b). Specifically, we conduct a 1D simulation as in Morris & Desch (2010), based on Desch & Connolly (2002), including emission, absorption, and transfer of continuum radiation from solids, and the molecular radiation from H_2O, dissociation and recombination of H_2 molecules, and evaporation of small particles. However, we replace the 1D radiation field J seen by chondrules with one that is a mixture of the local 1D radiation field and the radiation field they see from the cool gas on the other side of the bow shock. To calculate this mixed radiation field, we consider chondrules to lie in one of two semi-infinite spaces separated by a plane, which represents the bow shock. As seen in Figure 3 (right), chondrules tend to move very close, and parallel to the shock front. We assume they all remain at a fixed optical depth τ from the bow shock. On the unshocked side of the bow shock, we assume the temperature is that of the background nebula, $T_{bkgrnd} \approx 150\,\text{K}$. On the other side lies heated chondrules, and the hot ($T \sim 10^3\,\text{K}$) gas in the planetary embryo's wake. The column density across the wake region is $\sim 10\,\text{g cm}^{-2}$, which for a solar-composition gas yields a column density of water molecules $N_{H2O} \sim 10^{21}\,\text{cm}^{-2}$, which is optically thick in the infrared (Morris et al. 2009). In addition, gas that might contain dust is mixed into the wake region, especially at $Y > +8000\,\text{km}$. This justifies the assumption of a semi-infinite space at high temperature, which we assume is the local temperature of chondrules, T_{ch}. Making these assumptions, it is straightforward to show that chondrules see a radiation field with mean intensity,

$$J(\tau) = B(T_{ch}) + \frac{1}{2}[B(T_{bkgrnd}) - B(T_{ch})]\, E_2(\tau), \qquad (9)$$

where B is the Planck radiation function and E_2 is the second exponential integral.

We replace the radiation field seen by chondrules with this quantity, where τ is an input parameter describing the optical depth between the chondrules and the gas. We note that the previous work of Morris et al. (2010a, 2010b) differed in two ways. In that work, $E_2(\tau)$ was approximated by $\exp(-\tau)$, which is a reasonably good assumption. That work also assumed the wake of the planetesimal was *not* optically thick, so that $\exp(-\tau)$ was used instead of the more appropriate $E_2(\tau)$ used here. Because of these differences, cooling rates are roughly
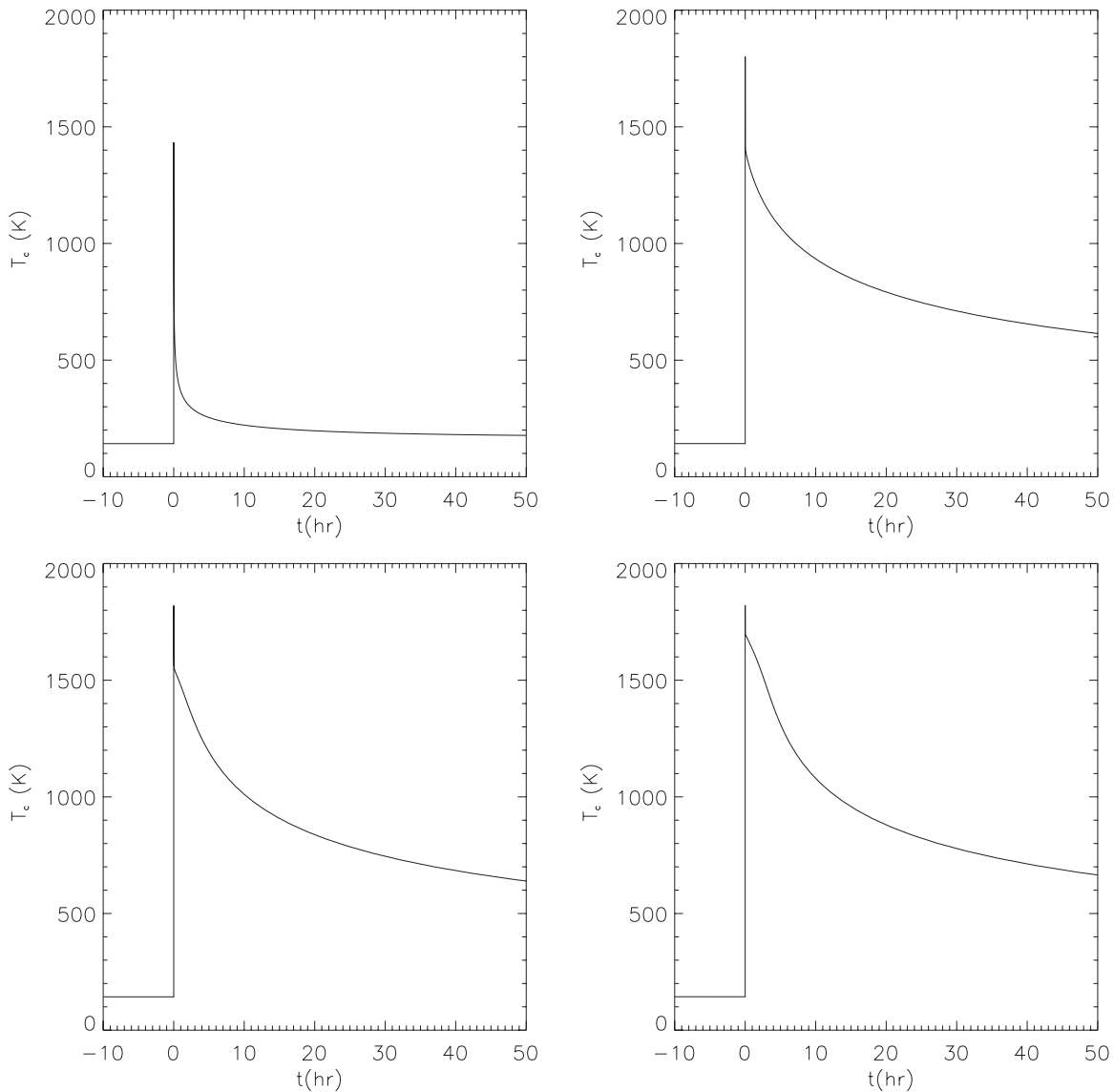
Figure 5. Thermal histories of chondrules formed in bow shocks around planetary embryos, assuming shock speeds of $5\,\mathrm{km\,s^{-1}}$ (top left), $6\,\mathrm{km\,s^{-1}}$ (top right), $7\,\mathrm{km\,s^{-1}}$ (bottom left), and $8\,\mathrm{km\,s^{-1}}$ (bottom right). Chondrule precursors pass through the shock front at $t = 0$. See the text for details.

an order of magnitude slower here than found by Morris et al. (2010a, 2010b). As discussed above in Section 3, we consider $\tau = 0.16$ to be a typical value for those particles that melt as chondrules (impact parameters from 400 to 4300 km), provided $\mathcal{C} \approx 10$. Based on this, $E_2(0.16)/2 = 0.313 = \exp(-1.16)$, meaning that the radiation field seen by chondrules is roughly 69% the radiation field they would normally see in the 1D shock, mixed with 31% of the background radiation field. Chondrules are warmed by the radiation field from nearby chondrules, but not as much as they would be in a 1D shock.

We now consider the possible effects of H_2O line cooling in this case. Morris & Desch (2010) found that molecular line cooling due to H_2O was negligible in large-scale shocks, due to the combined effects of high column densities of water seconds after the shock, backwarming, and, most importantly, H_2 recombinations. However, we must consider whether line cooling would become significant in the geometry of a bow shock. Recall from above that the column density of water molecules across the wake region is $N_{\mathrm{H2O}} \sim 10^{21}\,\mathrm{cm^{-2}}$, so the region is optically thick to line photons shortly after the shock

(Morris et al. 2009). Not only is the wake region optically thick to line photons, but the high column density of water also tends to block continuum radiation escaping through the wake region. Although the effects of backwarming may be reduced somewhat due to the bow shock geometry, buffering by H_2 recombinations will be unaffected. The combination of high column densities of water and buffering by H_2 recombinations will dominate over any reduction in the efficiency of backwarming due to the geometry. Therefore, we still consider H_2O line cooling negligible in bow shocks.

In Figure 5, the thermal histories of chondrules are shown for four possible values of the shock speed: $V_s = 5\,\mathrm{km\,s^{-1}}$, $6\,\mathrm{km\,s^{-1}}$, $7\,\mathrm{km\,s^{-1}}$, and $8\,\mathrm{km\,s^{-1}}$. In each case chondrules are heated by absorbing infrared radiation emitted by other chondrules in the vicinity, by thermal exchange with the gas in the post-shock region, and by frictional heating in the minute or so past the shock where the chondrules move at supersonic speeds V_{rel}, with respect to the gas. As described above, the radiation field seen by chondrules has been artifically lowered from the radiation field they would normally see, using the factor $\tau = 0.1$ ($\tau' = 1$). The peak temperature is sensitive

to the supersonic heating rate, which scales as V_{rel}^3 (up to the liquidus temperature), and strongly correlates with shock speed. We find $T_{\text{peak}} \approx 1430\,\text{K}$ for $V_s = 5\,\text{km s}^{-1}$, $T_{\text{peak}} \approx 1800\,\text{K}$ for $V_s = 6\,\text{km s}^{-1}$, $T_{\text{peak}} \approx 1820\,\text{K}$ for $V_s = 7\,\text{km s}^{-1}$, and $T_{\text{peak}} \approx 1820\,\text{K}$ for $V_s = 8\,\text{km s}^{-1}$. Note that thermal histories become increasingly uncertain for times $>5\,\text{hr}$ (i.e., for temperatures $<1400\,\text{K}$) because the assumption of a 1D geometry becomes increasingly less valid.

Chondrule peak temperatures must exceed 1770–2120 K to produce porphyritic textures (Hewins & Connolly 1996; Desch & Connolly 2002). Formation of chondrules therefore requires $V_s \gtrsim 6\,\text{km s}^{-1}$, or $V_{\text{rel}} \gtrsim 5\,\text{km s}^{-1}$. For the runs where peak temperatures were sufficient to melt the chondrules, the cooling rates through the crystallization temperature range ($\approx$1400–1820 K; Desch & Connolly 2002) were $<10^2\,\text{K hr}^{-1}$ (the cooling rate for chondrules in the shock with $V_s = 6\,\text{km s}^{-1}$ did not begin to cool slowly until their temperatures dropped below 1400 K). If we repeat our calculations with $\mathcal{C} \gtrsim 100$, we recover the optically thick, 1D limit for which cooling rates are $<10^2\,\text{K hr}^{-1}$. If we reduce $\mathcal{C}$ below 10, the chondrule cooling rates increase. They may not increase significantly if the wake region remains optically thick, but if it does not, then $\mathcal{C} \sim 1$ leads to cooling rates $\sim 10^3\,\text{K hr}^{-1}$ (Morris et al. 2009). From all this, we conclude that both peak temperatures and cooling rates are consistent with formation of porphyritic textures of chondrules, provided shocks speeds are $V_s > 6\,\text{km s}^{-1}$ ($V_{\text{rel}} > 5\,\text{km s}^{-1}$), and $\mathcal{C} > 10$. Lower particle concentrations may also be consistent with cooling rates $<10^3\,\text{K hr}^{-1}$, although we have not tested this. The required shock speeds are obtained so long as the planetary embryo has sufficient orbital eccentricity and/or inclination.

Because cooling rates are sensitive to chondrule concentrations $\mathcal{C}$, it is worth considering likely values of $\mathcal{C}$ as well as the length scales over which such concentrations are achieved. One mechanism that may lead to a high concentration of chondrules is settling to the midplane, which is inferred observationally in certain young protoplanetary disks (Furlan et al. 2011). In this scenario, the level of turbulence at the midplane is low enough that chondrules have a scale height h_c significantly smaller than the scale height H of the gas. Dubrulle et al. (1995) calculated the scale height of particles as a function of the level of turbulence, as parameterized by α. This can be written in terms of $\mathcal{S} = \alpha/(\Omega\, t_{\text{stop}})$, where Ω is the Keplerian orbital frequency, $t_{\text{stop}} = \rho_s a_c/\rho_g c_s$ is the chondrules' aerodynamic stopping time as defined in Section 3, $\nu = \alpha c_s H$ is the turbulent viscosity, c_s is the sound speed of the gas, and $H = c_s/\Omega$. The chondrule scale height is

$$h_c = h\left[1 + \left(\frac{h}{H}\right)^2\right]^{-1/2}, \qquad (10)$$

where $h/H = (\gamma + 1)^{-1/4}\mathcal{S}^{1/2}$. If $\alpha \ll \Omega\, t_{\text{stop}}$, then $h \ll H$ and chondrules may be concentrated at the disk midplane. Assuming $\rho_g = 1 \times 10^{-9}\,\text{g cm}^{-3}$, $C = 0.7\,\text{km s}^{-1}$ ($T = 150\,\text{K}$), and $\Omega = 7 \times 10^{-8}\,\text{s}^{-1}$ ($r = 2\,\text{AU}$), $t_{\text{stop}} = 1400\,\text{s}$ and $\Omega\, t_{\text{stop}} = 1 \times 10^{-4}$. If $\alpha \ll 10^{-4}$ then chondrules will concentrate to the midplane.

If the turbulent viscosity of the disk is dominated by magnetorotational instability, it is possible, but not certain, that α may be low enough at the midplane to allow chondrules to settle. Even low values of α are insufficient to allow chondrules to settle: for $\alpha = 1 \times 10^{-4}$, $\mathcal{S} = 1$, $h/H = 0.8$ (for $\gamma = 1.4$), and $h_c = 0.8H$, signifying relatively good mixing of chondrules

with the gas. To obtain $\mathcal{C} = 10$ requires $\alpha < 1.6 \times 10^{-6}$, so that $\mathcal{S} < 1.6 \times 10^{-2}$, $h/H < 0.101$, and $h_c < 0.100H$, implying significant settling to the midplane. Chondrule concentrations would then be 10 times their background nebular values, over a thickness $\lesssim H/10$.

This analysis is complicated by the possibility that a significant fraction of the solid's mass may be locked up in large planetesimals. If half of the solid's mass is locked up in planetesimals, the same optical depths in the chondrule-forming region require chondrules to be concentrated by a factor of 20 instead of 10, which would require $\alpha < 3.9 \times 10^{-7}$ so that $h/H < 2.5 \times 10^{-3}$ and $h_c < 0.050H$. If 90% of the solid's mass is locked up in planetesimals, the same optical depths would require a concentration by a factor of 100 instead of 10, which would require $\alpha < 1.6 \times 10^{-8}$ so that $h_c < 0.010H$. It is not clear what value of α is appropriate at the midplanes of protoplanetary disks in which the magnetorotational instability cannot act at the midplane. In principle, lower values are possible (e.g., Turner et al. 2010), but values $\alpha \approx 10^{-4}$ are thought to be appropriate (Fleming & Stone 2003), which would make it difficult for significant concentrations of chondrules to be achieved.

Turbulence itself provides a second mechanism for concentrating chondrules. Cuzzi et al. (2001) demonstrated that particles with an aerodynamic stopping time equal to the turnover time of the Kolmogorov-scale eddies can be concentrated in the stagnant zones between turbulent eddies. Particles with this stopping time have a size,

$$a_c = \frac{\rho_g c_s \nu_m^{1/2}}{\rho_s \Omega (\alpha c_s H)^{1/2}}. \qquad (11)$$

The molecular viscosity $\nu_m = \eta/\rho_g$, where η is given by Sutherland's formula. Following the discussion in Desch (2007), and assuming a solar composition gas with $T = 150\,\text{K}$ and the parameters above, we calculate $\eta = 59\,\mu\text{P}$ and $\nu_m = 5.9 \times 10^4\,\text{cm}^2\,\text{s}^{-1}$. For $\alpha = 10^{-4}$ we determine that the size of particles necessary for concentration is $a_c = 280\,\mu\text{m}$. Chondrule precursors with a radius of $300\,\mu\text{m}$, as we have assumed in our model, have almost the exact size to be optimally concentrated. Particle concentrations $\mathcal{C} \sim 10$ are easily achieved (Cuzzi & Hogan 2003).

Even if a significant fraction of the mass of solids is locked up in large planetesimals, there will be many regions in the nebula that have these concentrations of chondrule precursors. For example, in nebular gas with $\alpha = 10^{-4}$, nearly 80% of all chondrule precursors are in regions where their densities are concentrated by factors of 10 above background values, 70% are in regions with concentrations 20 times their background density, and 20% are in regions with concentrations 100 times their background density (Cuzzi et al. 2001). Of course, only small fractions of the *volume* of the nebula see concentrations this high, but these regions are where most chondrule precursors reside. The length scale over which a concentration $\mathcal{C}$ is achieved roughly scales as $(10^6\,\text{km})/\mathcal{C}$ (Cuzzi & Hogan 2003), so even regions with $\mathcal{C} = 100$ are $>10^4\,\text{km}$ in extent and thus are wider than the planetary embryo bow shock itself. We are justified in assuming a uniform value of $\mathcal{C}$ when computing chondrule thermal histories. Note that while a planetary embryo will pass through clumps with $\mathcal{C} = 10$–100, with sizes 10^5–$10^4\,\text{km}$, in only 3–0.3 hr, the newly formed chondrules remain in the vicinity of each other. To fix ideas, we assume that half of the solids mass is locked in large planetesimals, so that the optical depths assumed in the thermal histories above requires

concentrations by factors of 20, which are achieved over regions 50,000 km in extent, which contain 70% of all chondrule precursors. If the planetary embryo is on an orbit eccentric and/or inclined enough to yield shock speeds $>6\,\mathrm{km\,s^{-1}}$, the chondrule precursors in these clumps would be melted and would cool in a manner consistent with the dominant porphyritic textures.

5. CHEMICAL ENVIRONMENT OF PLANETARY EMBRYO BOW SHOCKS

We now consider the formation environment experienced by chondrules in bow shocks around planetary embryos, which we expect to be quite different from the environment in planetesimal bow shocks. Dauphas & Pourmand (2011) have suggested that Mars accreted roughly half its mass within $1.8^{+0.9}_{-1.0}$ Myr after the formation of CAIs. It therefore must have contained abundant live ^{26}Al when it formed, sufficient to melt the planet (Dauphas & Pourmand 2011; Grimm & McSween 1993). It is presumed that such a body would also form a magma ocean, convect, and rapidly outgas volatile species. Zahnle et al. (2007) have considered the outgassing of volatiles from the Earth following the Moon-forming impact, when the Earth was in its magma ocean state, and concluded that an atmosphere in chemical equilibrium with the magma could rapidly develop in $<10^3$ yr. Elkins-Tanton (2008) showed that the mantle of an Earth-sized planet takes 5 Myr to become 98% solidified. This suggests that planetary embryos could maintain a magma ocean and outgas volatile species for several Myr, perhaps aided by the continuous decay of ^{26}Al.

The composition of the planetary embryo's atmosphere probably was similar to Earth's outgassed atmosphere during its magma ocean stage. Zahnle et al. (2007) considered the atmosphere outgassed from the proto-Earth's magma ocean. They calculated that a fraction of Earth's CO_2 would be outgassed, equivalent to a partial pressure $P_{CO2} \approx 100$ bar, and that a substantial fraction of the H_2O would be outgassed too, equivalent to a partial pressure $P_{H2O} \approx 100$ bar. Other moderately volatile species such as S, Na, Zn, Cl and K are also expected to be outgassed during the magma ocean stage (Zahnle et al. 2007; Holland 1984).

We estimate the abundances of these species in the atmosphere of the planetary embryo by assuming that while outgassing may continue for many Myr, at any one instant in time the magma ocean is in chemical equilibrium with the atmosphere. The mass fraction of CO_2 dissolved in the magma scales linearly with the partial pressure in the atmosphere, as

$$x_{CO2} = 4.4 \times 10^{-7} \left(\frac{P_{CO2}}{1\,\mathrm{bar}} \right) \qquad (12)$$

(Stolper & Holloway 1988). It is straightforward to show that if the planetary embryo has the same total abundance of CO_2 (C) that P_{CO2} will scale as g^2, where g is the gravitational acceleration at the planet surface. We accordingly estimate $P_{CO2} \approx 10$ bar. The solubility behavior of N_2 is similar to that of CO_2 (Fricker & Reynolds 1968) and we assume $P_{N2} \sim 0.1$ bar. The mass fraction of water dissolved in the magma, x_{H2O}, is related to the partial pressure of water vapor in the atmosphere, P_{H2O}, by the relation

$$x_{H2O} = 6 \times 10^{-7} \left(\frac{P_{H2O}}{1\,\mathrm{dyn\,cm^{-2}}} \right)^{0.54} \qquad (13)$$

(Fricker & Reynolds 1968). Analyses of Martian meteorites have led to estimates of Mars's bulk water content in a range of 140–250 ppm (McCubbin & Elardo 2011), or 0.5wt% (Craddock & Greeley 2009) to $\approx$1.4–1.8wt% (McSween & Harvey 1993; McSween et al. 2001; Dann et al. 2001). We take a median value, $x_{H2O} = 0.2$wt%, as a representative value (a mass fraction equivalent to the Earth having eight oceans, in line with current estimates by Mottl et al. 2007), so that the total mass of H_2O in the planetary embryo is 6.6×10^{23} g, and $P_{H2O} = 3.3$ bar. Assuming $M_p = 3.31 \times 10^{26}$ g, $R_p = 2720$ km, and a gravitational acceleration $g = 300\,\mathrm{cm\,s^{-2}}$, we determine an equilibrium mass of H_2O in the atmosphere of 1.0×10^{22} g, which is a small fraction of the total mass. The equilibrium abundance of Na in the atmosphere is complicated by the fact that it may dissolve in the magma either as Na_2O or as NaOH, in which case its solubility is affected by the water content. van Limpt et al. (2006) considered Na solubility for silicate glasses and found the following relationship to hold when Na dissolves as NaOH (i.e., in the presence of H_2O):

$$P_{NaOH} \approx 1.2 \times 10^{-3} \left(\frac{P_{H2O}}{1\,\mathrm{bar}} \right)^{0.5} \mathrm{bar}. \qquad (14)$$

For $P_{H2O} = 3.3$ bar, we find $P_{NaOH} \approx 2 \times 10^{-3}$ bar. Altogether, we infer that if the bulk abundance of water on the planetary embryo is 0.2%, then the planetary embryo's atmosphere during the magma ocean stage is mostly (88wt%) CO_2 with partial pressure 10 bar, some (12wt%) H_2O with partial pressure 3.3 bar, and alkalis and volatiles being trace species, with Na having a partial pressure $\approx 2 \times 10^{-3}$ bar. The total mass of the atmosphere is $\approx 4 \times 10^{22}$ g.

This atmosphere will be continuously stripped by KH instabilities at the interface between the atmosphere and the post-shock gas streaming by the planet. We did not include such an outgassed atmosphere, but the primary atmosphere accreted by the planetary embryo in our simulations plays the same role. The stripping by KH rolls at the interface between the planetary atmosphere and the post-shock gas, in particular, is expected to follow the same general trends. We find using dye calculations (see Section 2) that the atmosphere is lost at a rate $\approx 2 \times 10^{12}\,\mathrm{g\,s^{-1}}$, about 1% of the rate at which the planetary embryo intercepts nebular gas. This is in line with similar rates of KH stripping in other examples of strongly bound gas (e.g., around protoplanetary disks; Ouellette et al. 2007). This is sufficiently rapid to deplete the atmosphere after about 600 years, but outgassing can continue to replenish the atmosphere as the magma ocean convects (on shorter timescales) and bring new volatiles to the surface. The planetary inventory of water, in particular, in this example could persist for 8×10^4 yr. The reservoirs of Na and other species would persist for many Myr.

Not only are gases from the planetary embryo's atmosphere stripped by KH rolls at the interface with the shocked gas, as seen in Figure 3; chondrules also make excursions in and out of these rolls and this planetary gas. Chondrules will be exposed, at least some of the time, to volatiles such as H_2O and Na outgassed from the planetary embryo's magma ocean. The scale height of the atmosphere proper (which has been shocked to $\approx$2500 K) is approximately 185 km, so even at the 800 km distance between the planetary surface and the boundary layer at the top of the atmosphere, gas pressures should be $\sim$1% of their values at the surface. We estimate $P_{H2O} \sim 3 \times 10^{-2}$ bar and $P_{Na} \sim 2 \times 10^{-5}$ bar. Chondrules passing through KH rolls

will experience approximately these partial pressures of volatile species.

It is important to note that when we calculated approximate chondrule thermal histories in Section 4, we assumed the only gas to which chondrules were exposed was the shocked nebula gas, with pressure $\sim 10^{-3}$ bar. If chondrules pass in and out of the plumes of planetary atmosphere gas in KH rolls, they will see much higher pressures, $\sim 10^{-1}$ bar. This could potentially affect chondrule thermal histories in two ways: during the first minute past the shock front, higher gas densities can more rapidly decelerate the chondrule and heat it by friction; and thermal exchange with the hot gas will become more efficient. Neither of these effects is likely to drastically alter the thermal histories of the chondrules considered here, because nearly all of the chondrule deceleration takes place in the shocked nebula gas during the first minute, outside of the planetary atmosphere (see Figure 3 (right)). Also, the denser plumes of gas are not likely to be at significantly different temperatures, and chondrule temperatures will be dominated by radiative effects. A full treatment of chondrule thermal histories in future work must more fully consider these effects.

Elevated partial pressures of volatiles may explain puzzling features of the chondrule formation environment. An enhanced abundance of water vapor is potentially consistent with indicators of elevated oxygen fugacity during chondrule formation (Krot et al. 2000; Fedkin & Grossman 2006; Grossman et al. 2011). Partial pressures $P_{H2O} > 10^{-3}$ bar have been suggested to explain the fayalite content of chondrule olivine (Fedkin & Grossman 2006). Likewise, the high partial pressure of Na vapor may potentially explain the finding by Alexander et al. (2008) that olivine phenocrysts in chondrules from Semarkona contain ~ 0.010–0.015 wt% Na_2O, even at their cores, strongly implying that Na was dissolved in the melt as the olivine crystallized. Alexander et al. (2008) expressed the needed partial pressures in terms of a density of solids, assuming that the Na derived from the chondrule melts and that 10% of this Na entered the gas phase. Their inferred chondrule densities ranged from low values up to at least ≈ 400 g m^{-3}. Assuming the chondrule is 0.01 wt% Na_2O, this implies an Na vapor density of 3×10^{-9} g cm^{-3} and a partial pressure of Na $\approx 2 \times 10^{-5}$ bar. Remarkably, the volatiles escaping from the planetary embryo's magma ocean and mixing with the post-shock gas may provide the partial pressures of H_2O and Na assumed to have been experienced by chondrules.

We have not modeled in detail the production of a secondary atmosphere, nor quantified in detail how that atmosphere is stripped, or how often chondrules encounter this stripped gas. We have demonstrated that chondrules do make excursions into gas that is strongly bound to the planet, and that this gas may contain elevated abundance of species outgassed during a planet's magma ocean stage, including H_2O, CO_2, Na, and K vapor, in particular. Our best estimates of the partial pressures of water vapor and Na vapor are consistent with values needed to provide an environment with elevated oxygen fugacity and the ability to suppress evaporation of alkalis, although our results depend on the assumption $x_{H2O} = 0.2$ wt%. Further tests are required to better test these ideas quantitatively.

6. MASSES OF CHONDRULES FORMED BY PLANETARY EMBRYO BOW SHOCKS

A very large number of chondrules can be produced by a single planetary embryo on an eccentric and/or an inclined orbit. Chondrules will be produced as long as the velocity difference

between the body and the gas is $V_s \gtrsim 6$ km s^{-1}, which requires the eccentricity e and inclination i of the body to be sufficiently large. Over time, however, the interaction of a planetary embryo with nebular gas will cause its eccentricity and inclination to damp to low values. The total number of chondrules produced depends on the e and i damping timescales. In this section we construct a model for estimating the orbital conditions, duration, and mass processed during a single scattering event. The model includes e and i damping due to gas drag and disk torques, as well as semimajor axis evolution due to energy dissipation from drag. Migration due to torques is ignored for convenience and to reflect the fact that the magnitude and *direction* of migration can differ depending on the equation of state (e.g., Paardekooper & Mellema 2006) and on whether radiative transfer is included or not (e.g., Bitsch & Kley 2010). Below, we discuss the methods for including torques and drag, in turn, and then combine them to estimate the orbital evolution and mass of chondrules processed.

6.1. Eccentricity Damping of Planetary Embryos

We first consider eccentricity damping by torques. Recent simulations by Cresswell et al. (2007) and Bitsch & Kley (2010) demonstrate that eccentric planets in radiatively cooling disks follow analytic limits. When the eccentricity e is high, $de/dt|_h = -K_e e^{-2}$ (Papaloizou & Larwood 2000), where K_e is a constant. When e is low, de/dt follows an exponential decay that is well characterized by $de/dt|_\ell = -e/t_{ecc} = -e\,0.78\,q\,(\Sigma a^2/M_*)h^{-4}\Omega$, where q is the planet-to-star mass ratio, a is the planet's semimajor axis, M_* is the mass of the star, $h = H/a$ for scale height $H(a)$ at heliocentric distance a, $\Sigma(a)$ is the total surface density at heliocentric distance a, and $\Omega(a)$ is the average angular speed of the planet (Tanaka & Ward 2004). The low-e limit is valid for $e \lesssim 0.1$. Using these results, we explore parameter space without using costly hydrodynamics simulations by making the *ansatz* that the total rate is the harmonic sum of the limits, such that $de/dt = -K_e e/(K_e t_{ecc} + e^3)$. We select a family of solutions by varying only K_e and assuming that $K_e t_{ecc}$ is a constant over the parameter space of interest. Based on Cresswell et al. (2007) we set $K_e t_{ecc} = 0.00253$, which allows us to match their eccentricity evolutions.

For the inclination evolution, the rates follow the same limiting behavior as in eccentricity damping, with $di/dt|_\ell = -i/t_{inc} = -i\,0.544\,q\,(\Sigma a^2/M_*)h^{-4}\Omega$ (Tanaka & Ward 2004) and $di/dt|_h = -K_i i^{-2}$ (Bitsch & Kley 2011). Based on the simulations of Bitsch & Kley (2011), we make the same assumptions for the total inclination damping as we have made for the eccentricity damping, and we vary K_i while keeping constant $K_i t_{inc} = 0.00075$. Strictly speaking, the inclination and eccentricity damping are coupled, but they are treated independently for the estimates we present here.

For disk torques, we neglect dynamical friction between the embryo and a sea of planetesimals, which is given by $de/dt|_{DF} = -\ln(1 + \Lambda^2)G\Sigma_p q/(\sqrt{2}\Omega ae^3)$ (Ford & Chiang 2007). Here, Σ_p is the surface density of planetesimals and the natural log term is the Coulomb parameter. The ratio $(de/dt|_\ell)/(de/dt|_{DF}) \approx (e/h)^4 \Sigma/\Sigma_p(\ln(1 + \Lambda^2))^{-1}$. For typical parameters ($\Sigma/\Sigma_p \sim 100$, $\ln(1 + \Lambda^2) \sim 10$, and $h \sim 0.05$) dynamical friction is unimportant until $e \sim 0.03$. We show below that chondrule-producing shocks are only achieved for $e \gtrsim 0.1$. Therefore, gas disk torques will dominate over dynamical friction.

Now we consider the effects of gas drag on large solids. Planetesimals and planets are much larger than the mean free path of gas molecules λ, so the drag is in the Stokes regime, i.e., the Knudsen number $\mathrm{Kn} \equiv 2R_p/\lambda \ll 1$. In this regime the gas drag takes the form $d(\delta v)/dt = -3\zeta \,\mathrm{Kn}\, k_d\, \delta v$, where δv is the velocity difference, k_d is a coupling coefficient, and $\zeta = (8/\pi)^{1/2}(\rho_g c_a)/(\rho_s R_p) = (8\gamma/\pi)^{1/2} t_{\mathrm{stop}}^{-1}$, where c_a is the adiabatic sound speed and t_{stop} and other quantities are defined as before. The coupling coefficient k_d depends on the Reynolds number $\mathrm{Re} = 3(\pi/8)^{1/2}\mathcal{M}/\mathrm{Kn}$, where $\mathcal{M} = \delta v/c_s$. In the regime of interest ($\mathrm{Re} > 1500$), $k_d = 0.11\,\mathrm{Re}$ (Paardekooper 2007). This yields $d(\delta v)/dt \approx -(\delta v)/t_{\mathrm{stop}}$ in accord with Adachi et al. (1976).

The evolution of the planetary embryo's orbit can now be determined if δv can be expressed as a function of e and i. In general δv will vary along the body's orbit, depending on the value of the true anomaly ϕ. We model the damping by solving Kepler's equation for following the orbit of a planet, and by using a predictor–corrector for modifying the eccentricity and inclinations over a time step. The time derivatives of the radial and tangential velocity components for a Keplerian orbit are

$$\frac{dv_\phi}{dt} = \left(\frac{\mu}{a(1-e^2)}\right)^{1/2}\left[\left(\frac{e}{1-e^2}(1+e\cos\phi)+\cos\phi\right)\frac{de}{dt} \right. \\ \left. - e\sin\phi\frac{d\phi}{dt}\right] \tag{15}$$

$$\frac{dv_r}{dt} = \left(\frac{\mu}{a(1-e^2)}\right)^{1/2}\left[\left(\frac{e^2}{1-e^2}+1\right)\frac{de}{dt}\sin\phi \right. \\ \left. + e\cos\phi\frac{d\phi}{dt}\right], \tag{16}$$

where $\mu = G(M_* + M_p)$. We find an expression for the change in eccentricity by keeping only the terms with de/dt, as the other terms represent the unaltered Keplerian orbit. This gives

$$\left(\frac{d\delta v}{dt}\right)^2 = \frac{\mu}{a(1-e^2)}\left(\frac{de}{dt}\right)^2\left[\left(\frac{e}{1-e^2}(1+e\cos\phi)+\cos\phi\right)^2 \right. \\ \left. + \left(\left(\frac{e^2}{1-e^2}+1\right)\sin\phi\right)^2\right]. \tag{17}$$

The change in eccentricity over time can thus be expressed in terms of the change of the relative velocity over a computational time step. A similar approach can be taken with the inclination, where $d(\delta v_z)/dt \approx (\mu/r_{\mathrm{cyl}})^{1/2}\, di/dt$, where r_{cyl} is the projected radial separation. We have assumed small i here because drag predominantly takes place within one scale height of the disk, and we in fact only include drag when $|z| < H$. Finally, we use the energy gained or dissipated in a time step, δE, to computed an updated semimajor axis $a = -(\mu/2)(E + \delta E)^{-1}$.

We now apply these formulae to conditions in protoplanetary disks. In our orbital damping calculations we use a disk model with gas surface density $\Sigma(r) = 149\,(r/5.2\,\mathrm{AU})^{-1.5}\,\mathrm{g\,cm^{-2}}$, a gas scale height $H = 0.05r$, a midplane density $\rho_0 = \Sigma/(2H)$, and a stellar mass of $1\,M_\odot$. To illustrate which damping terms are most important, we plot in Figure 6 the eccentricity damping timescale $e\,(de/dt)^{-1}$ as a function of planetary mass M_p, for our model conditions and with $e = 0.4$ and $i = 0°$. The internal density in this example was set to be $\rho_s = 5.7\,\mathrm{g\,cm^{-3}}$, appropriate for Earth-like bodies but slightly denser than our
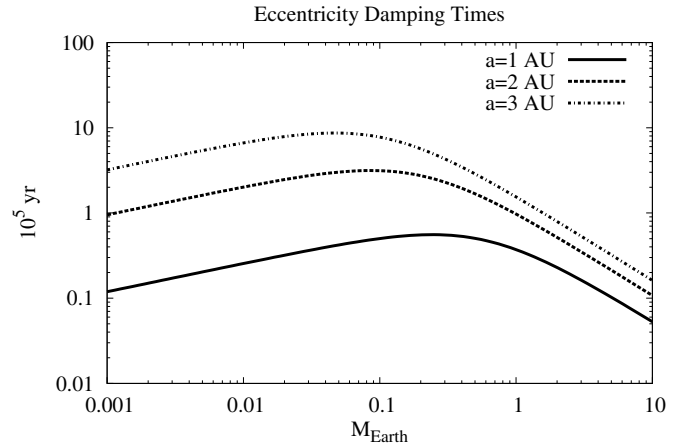
Figure 6. Eccentricity damping times as a function of planetary embryo mass. Damping for small bodies ($M < 0.1\,M_\oplus$) is dominated by gas drag, and damping of large bodies ($M > 1\,M_\oplus$) is dominated by disk torques. For heliocentric distances 1–3 AU, Mars-sized bodies are in the transition regime that is least damped.

proto-Mars planetary embryo. Each curve represents damping at pericenter for different a. In Figure 6 it is seen that bodies with small mass ($M_p < 0.1\,M_\oplus$) are in the drag-dominated regime, with damping timescales that increase with increasing mass as $M_p^{1/3}$. Bodies with large mass ($M_p > 1\,M_\oplus$) are in the disk torque regime, with damping timescales that decrease as the planet's mass is increased, roughly as M_p^{-1}. The transition between these regimes, and the maximum damping timescales $\sim 10^5$ yr, occurs for bodies of mass approximately 0.1–0.2 $M_\oplus$, somewhat larger than the planetary embryo we consider ($= 0.055\,M_\oplus$).

In Figure 7, we show the eccentricity evolution of a scattered planetary embryo with mass $M_p = 0.055\,M_\oplus$ and $R_p = 2720$ km. The semimajor axis a is set to 2.5 AU, but various starting eccentricities e_0 and inclinations i_0 for strong scattering events are explored. These plots demonstrate that for plausible scattering scenarios the planetary embryo retains high eccentricity for a few $\times 10^5$ yr. More relevantly, the maximum shock speeds are shown to exceed the critical value ($\approx 6\,\mathrm{km\,s^{-1}}$) for 1–4×10^5 yr, if $e_0 = 0.4$, and for a shorter time if $e_0 = 0.2$.

Although the large eccentricities and inclinations explored here may not be common, they do represent values that could be met repeatedly during the lifetime of a disk (e.g., Chambers 2001; Hansen 2009).

6.2. Mass of Chondrules Produced per Embryo

We now calculate the mass of chondrules, M_c, produced by a single planetary embryo. The rate at which chondrules are processed over time is $dM_c/dt = \sigma\,V_s\,\rho_c$, where σ is the cross-section, which we set to $\pi(4300\,\mathrm{km})^2$ for the planetary embryo described in Section 2. The density of chondrule (precursors) is defined to be $\rho_c = f\,\mathcal{C}\rho_g$, with $f = 3.75 \times 10^{-3}$. The concentration factor of chondrules, $\mathcal{C}$, is a local value that can vary spatially throughout the disk due to settling or turbulence. The instantaneous velocity difference between the planetary embryo and the gas is V_s, which is also the shock speed. If $V_s < 6\,\mathrm{km\,s^{-1}}$ (or greater than $8\,\mathrm{km\,s^{-1}}$) it is assumed that chondrules are not melted (or are completely vaporized), and we set $dM_c/dt = 0$ for that part of the protoplanet's orbit. We calculate the total mass produced by integrating dM_c/dt over individual orbits and over the entire damping history of the protoplanet.
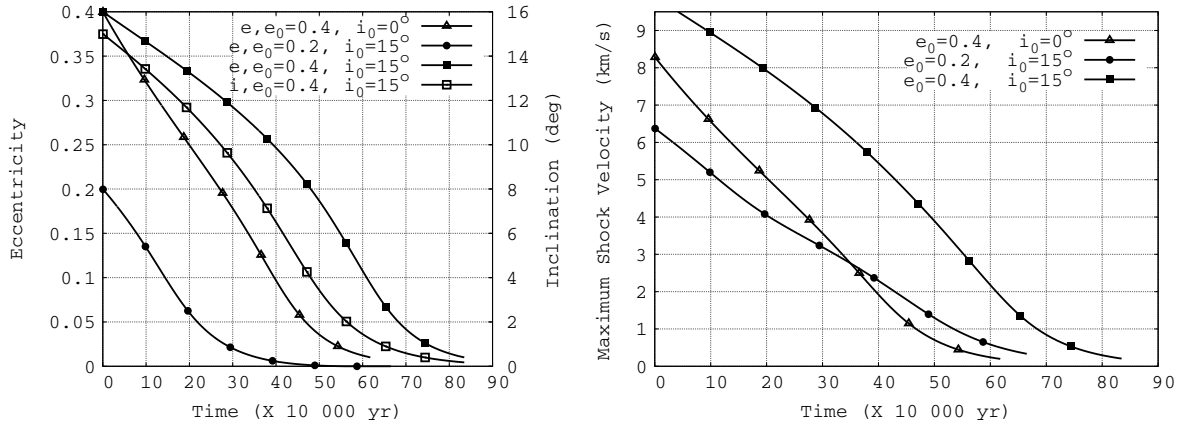
Figure 7. Left: eccentricity evolution for three scattered-planet scenarios. Each embryo has mass 0.055 $M_\oplus$, radius 2720 km, and semimajor axis 2.5 AU. Curves correspond to starting conditions $e_0 = 0.4$, $i_0 = 0°$ (solid triangles), $e_0 = 0.2$, $i_0 = 15°$ (solid circles), and $e_0 = 0.4$, $i_0 = 15°$ (solid and open squares). Right: maximum shock velocities during an orbit, as a function of time, for the same three cases.

Table 1
Chondrule Production in Planetary Embryo Bow Shocks

a_0 (AU)	e_0	i (deg)	V_s (km s^{-1})	M_c ($M_\oplus$)	Duration (yr)
1	0.1	0	3.0	...	...
1	0.2	0	6.1	8.3(−7)	1000
1	0.3	0	9.4	7.4(−5)	21000
1	0.4	0	13	1.1(−4)	29000
1	0.1	7	4.8	...	...
1	0.2	7	7.2	2.5(−5)	12000
1	0.3	7	10.2	6.5(−5)	24000
1	0.4	7	13.7	7.4(−5)	22000
1	0.1	15	8.4	4.6(−5)	43000
1	0.2	15	10.1	3.7(−5)	31000
1	0.3	15	12.5	3.6(−5)	25000
1	0.4	15	15.6	4.3(−5)	22000

Notes. Over the orbital evolution of the body, assuming an initial semimajor axis of $a = 1.0$ AU and different initial values eccentricity e and inclination i. We assume that chondrule formation occurs only when the instantaneous velocity difference V_s between the embryo and the gas is in the range $6 - 8$ km s^{-1}. Max V_s is the maximum shock velocity during the orbital evolution. The duration signifies the time period beginning with the first episode of chondrule formation and ending with the last episode of chondrule formation before damping of the embryo's e and i. A concentration factor $\mathcal{C} = 1$ (implying chondrules-to-gas mass ratio 0.00375) was assumed. Only material that is within $H/\mathcal{C}$, for disk gas scale height H is included in M_s. The notation $a(-b)$ means $a \times 10^{-b}$.

Tables 1–6 list the masses of chondrules produced in bow shocks around planetary embryos with a variety of initial semimajor axes a, eccentricities e, and inclinations, i. Based on the need to have $\mathcal{C} \gtrsim 10$ to match chondrule cooling rates (see Section 4), we consider two situations: one in which chondrules are locally concentrated by turbulence and one in which chondrules have settled to the midplane. We first consider the case where chondrules are concentrated via turbulence. As discussed in Section 4, chondrules more often than not find themselves in regions of enhanced chondrule density ($\mathcal{C} > 10$). As seen from the planetary embryo, which randomly samples all volumes of the disk, the average density of chondrules is $\mathcal{C} = 1$. Tables 1–3 list the masses of chondrules produced assuming $\mathcal{C} = 1$. We next consider the case where chondrules have settled to the midplane, by setting $\mathcal{C} = 10$ if $|z| < H/10$, and $\mathcal{C} = 0$ for z farther from the midplane. Tables 4–6 list the masses of chondrules produced assuming this form of $\mathcal{C}$. It is important

Table 2
Chondrule Production in Planetary Embryo Bow Shocks

a_0 (AU)	e_0	i (deg)	V_s (km s^{-1})	M_c ($M_\oplus$)	Duration (yr)
1.5	0.1	0	2.5	...	...
1.5	0.2	0	5.0	...	...
1.5	0.3	0	7.7	3.7(−5)	32000
1.5	0.4	0	11	8.8(−5)	64000
1.5	0.1	7	3.9	...	...
1.5	0.2	7	5.9	...	...
1.5	0.3	7	8.3	5.1(−5)	55000
1.5	0.4	7	11	6.5(−5)	56000
1.5	0.1	15	6.9	1.3(−5)	37000
1.5	0.2	15	8.2	2.7(−5)	68000
1.5	0.3	15	10	2.9(−5)	63000
1.5	0.4	15	13	3.6(−5)	58000

Note. Same as Table 1, but for $a = 1.5$ AU.

to note that these masses will be reduced if a large fraction of the solid's mass is locked up in large planetary bodies. A lower solids-to-gas ratio would also result in higher chondrule cooling rates, due to lower optical depth, but probably not significantly so; we expect them to remain within the range consistent with chondrule formation ($10-10^3$ K hr^{-1}).

As Tables 1–6 demonstrate, a single planetary embryo can produce a mass of chondrules close to the inferred present-day mass of chondrules, $\approx 2 \times 10^{-4}$ $M_\oplus$ (Grossman 1988). Higher initial eccentricities and lower initial inclinations favor greater chondrule formation in both concentration scenarios. Note that when planetary bodies are scattered out of the plane of the disk, the potential chondrule-forming *duration* is greatly extended because gas drag is only effective near the orbital nodes; however, chondrules would only be produced at the orbital nodes, so the longer duration does not necessarily equate to more mass processed. Comparing the cases where chondrules are concentrated by turbulence versus settled to the midplane, the total mass of chondrules is comparable when the planetary embryo has high inclination, whereas if the inclination is low ($\lesssim 10°$), a greater mass of chondrules is produced when chondrules settle to the midplane. For $a = 1.5$ AU, $e_0 = 0.4$ and $i = 0°$, 9×10^{-5} $M_\oplus$ of chondrules are produced over 64,000 years for the turbulent concentration case. For the case where chondrules settle to the midplane, a factor of 10 more chondrules are produced.

Table 3
Chondrule Production in Planetary Embryo Bow Shocks

a_0 (AU)	e_0	i (deg)	V_s (km s^{-1})	M_c ($M_\oplus$)	Duration (yr)
2.5	0.1	0	1.9	. . .	. . .
2.5	0.2	0	3.9	. . .	. . .
2.5	0.3	0	5.97	. . .	. . .
2.5	0.4	0	8.3	5.5(−5)	140000
2.5	0.1	7	3.0	. . .	. . .
2.5	0.2	7	4.5	. . .	. . .
2.5	0.3	7	6.4	5.5(−6)	35000
2.5	0.4	7	8.7	5.5(−5)	180000
2.5	0.1	15	5.3	. . .	. . .
2.5	0.2	15	6.4	3.1(−6)	32000
2.5	0.3	15	7.9	2.2(−5)	180000
2.5	0.4	15	9.9	2.8(−5)	190000

Note. Same as Table 1, but for $a = 2.5$ AU.

Table 4
Chondrule Production in Planetary Embryo Bow Shocks

a_0 (AU)	e_0	i (deg)	V_s (km s^{-1})	M_c ($M_\oplus$)	Duration (yr)
1	0.1	0	3.0	. . .	. . .
1	0.2	0	6.1	8.3(−6)	1000
1	0.3	0	9.4	7.4(−4)	21000
1	0.4	0	13	1.1(−3)	29000
1	0.1	7	4.8	. . .	. . .
1	0.2	7	7.2	3.0(−5)	12000
1	0.3	7	10.2	6.5(−5)	17000
1	0.4	7	13.7	7.9(−5)	12000
1	0.1	15	8.4	4.6(−5)	40000
1	0.2	15	10.1	3.6(−5)	28000
1	0.3	15	12.5	3.6(−5)	22000
1	0.4	15	15.6	4.3(−5)	18000

Note. Same as Table 1, but assuming a concentration of chondrules $\mathcal{C} = 10$ within a height $|z| < H/10$ of the midplane.

Table 5
Chondrule Production in Planetary Embryo Bow Shocks

a_0 (AU)	e_0	i (deg)	V_s (km s^{-1})	M_c ($M_\oplus$)	Duration (yr)
1.5	0.1	0	2.5	. . .	. . .
1.5	0.2	0	5.0	. . .	. . .
1.5	0.3	0	7.7	3.7(−4)	32000
1.5	0.4	0	11	8.8(−4)	64000
1.5	0.1	7	3.9	. . .	. . .
1.5	0.2	7	5.9	. . .	. . .
1.5	0.3	7	8.3	6.9(−5)	47000
1.5	0.4	7	11	7.9(−5)	33000
1.5	0.1	15	6.9	1.5(−5)	37000
1.5	0.2	15	8.2	2.8(−5)	62000
1.5	0.3	15	10	2.9(−5)	56000
1.5	0.4	15	13	3.6(−5)	49000

Note. Same as Table 4, but with $a = 1.5$ AU.

Table 6
Chondrule Production in Planetary Embryo Bow Shocks

a_0 (AU)	e_0	i (deg)	V_s (km s^{-1})	M_c ($M_\oplus$)	Duration (yr)
2.5	0.1	0	1.9	. . .	. . .
2.5	0.2	0	3.9	. . .	. . .
2.5	0.3	0	5.97	. . .	. . .
2.5	0.4	0	8.3	5.5(−4)	140000
2.5	0.1	7	3.0	. . .	. . .
2.5	0.2	7	4.5	. . .	. . .
2.5	0.3	7	6.4	8.8(−6)	35000
2.5	0.4	7	8.7	7.4(−5)	130000
2.5	0.1	15	5.3	. . .	. . .
2.5	0.2	15	6.4	3.5(−6)	32000
2.5	0.3	15	7.9	2.4(−5)	180000
2.5	0.4	15	9.9	2.9(−5)	170000

Note. Same as Table 4, but with $a = 2.5$ AU.

Tables 1–6 assume a planetary embryo mass 0.055 $M_\oplus$. This may be close to the optimal mass for producing chondrules. Provided that the body is large enough to actually produce chondrules (i.e., it is not a planetesimal for which chondrules are accreted, but is a large planetary embryo), the cross-section σ scales roughly as R_p^2. The product of this cross-section and t_{damp} yields the total mass of chondrules produced. For small bodies whose damping is dominated by gas drag, the mass of chondrules that is produced scales linearly with M_p. For large bodies whose damping is dominated by disk torques, the mass of chondrules that is produced scales roughly as $M_p^{-1/3}$. In fact, the mass of chondrules that can be produced per embryo is optimal for Mars-sized bodies with $M_p \sim 0.1 M_\oplus$. Nevertheless, as long as the body is larger than about 1000 km in radius, a comparable amount (to within factors of three) of chondrules will be produced.

The chondrule masses produced per embryo are intriguingly close to the mass $2 \times 10^{-4} M_\oplus$, and in principle a single scattered planetary embryo could produce the entire present-day inventory of chondrules. Nevertheless, to produce the observed mass of chondrules several planetary embryos probably would be required. This is because some of the solid's mass is locked up in large bodies, making fewer chondrule precursors available for processing. Also, the present-day asteroid belt may have been depleted since it formed, meaning there were more chondrules originally, potentially by a factor of 100 (Weidenschilling et al. 1998). On the other hand, eccentric planetary embryos may be a common event. Even for the minimum-mass solar nebula mass distribution assumed above, the annulus between 1.5 and 2.5 AU would have contained ≈1.5 $M_\oplus$ of solids. If half of the mass was in small (chondrule-like) particles and half locked up in large planetary embryos, potentially ≈25 planetary embryos could exist in that one annulus alone.

Our calculations show that, given the right orbital parameters, chondrules can form over a range of heliocentric distances 1.0–2.5 AU. Chondrules embedded in a disk with even low levels of turbulence may be spread over length scales $\Delta r = 1$ AU in $\lesssim 10^5$ yr, assuming an alpha viscosity law $\nu = \alpha H^2 \Omega$ (where H is the gas scale height, Ω is the Keplerian orbital frequency and α is a dimensionless constant ≈10^{-2}; Hartmann et al. 1998). Chondrules produced at 1.0–2.5 AU will relatively quickly be spread throughout the present-day asteroid belt to be incorporated into chondrite parent bodies.

7. DISCUSSION AND SUMMARY

Following the recent discovery that a planetary embryo, the half-formed Mars, existed at the same time chondrules were forming (Dauphas & Pourmand 2011), we have been motivated to study chondrule formation in the bow shocks

of planetary embryos on eccentric orbits. We have calculated the hydrodynamics of gas flowing through the bow shock of a large (radius 2720 km) planetary embryo. In contrast to bow shocks around smaller planetesimals, an embryo acquires a substantial primary atmosphere from the solar nebula. A boundary layer exists between this atmosphere and the shocked gas flowing past the planetary embryo, and this layer is unstable to KH instabilities. The planetary embryo is likely to have a magma ocean (Dauphas & Pourmand 2011), and the secondary atmosphere outgassed from the magma ocean would behave similarly dynamically.

We have calculated the trajectories of chondrules through the planetary embryo bow shock, subject to gravitational and gas drag forces. We find that the relative velocity between chondrules and gas is sufficient to melt chondrules ($>5\,\mathrm{km\,s^{-1}}$, equivalent to shocks with speed $>6\,\mathrm{km\,s^{-1}}$) only for chondrules with impact parameter $b < 400\,\mathrm{km}$ around a 500 km radius planetesimal, or impact parameter $b < 4300\,\mathrm{km}$ around a 2720 km radius planetary embryo. We find that the dynamical coupling between chondrules and gas is not achieved until the chondrules have passed about 400 km past the bow shock. For a small planetesimal the bow shock stands only ≈ 100 km from the body, and chondrules are not well coupled to the gas. All chondrules with $b < 460\,\mathrm{km}$, including all those particles achieving peak temperatures of chondrules and melted as chondrules, are accreted onto the planetesimal. For a larger planetary embryo, the bow shock stands $\approx 1000\,\mathrm{km}$ off of the boundary with the atmosphere, and very few chondrules are accreted by the protoplanet, only those with $b < 400\,\mathrm{km}$ ($<1\%$ of the chondrules formed in the bow shock).

We have calculated the thermal histories of chondrules in a planetary embryo bow shock. Our calculation of thermal histories builds on the 1D algorithm of Morris & Desch (2010) with the substitution of Morris et al. (2010a, 2010b) for the radiation field to allow the chondrules to radiate to the cold, unshocked gas. We find that shock speeds $>6\,\mathrm{km\,s^{-1}}$ and optical depths between chondrules and the unshocked gas >0.1 are sufficient to melt chondrules and yield cooling rates through the crystallization temperature range $<100\,\mathrm{K\,hr^{-1}}$, consistent with formation of porphyritic textures. These optical depths, we calculate, require concentrations of chondrules $\mathcal{C} > 10$ above a presumed background density $3.75 \times 10^{-3}\,\rho_g$ for a gas density $\rho_g = 10^{-9}\,\mathrm{g\,cm^{-3}}$. These concentrations are achievable by chondrules settling to the midplane or turbulent concentration. Moreover, a concentration factor of $\mathcal{C} = 10$ yields a compound chondrule frequency in accord with observations. To achieve the same optical depths in bow shocks around planetesimals requires much higher concentrations of chondrules.

We find that chondrules formed in a planetary embryo bow shock pass through the KH rolls at the boundary between the shocked gas and the planetary atmosphere, and will be exposed to the atmosphere gas. This atmosphere is composed of nebular gas but will be dominated by volatiles outgassed from the protoplanet's magma ocean. We have estimated the composition of the secondary atmosphere outgassed from the protoplanet to be roughly 10 bars of CO_2, 3 bars of H_2O, and 2×10^{-3} bars of Na vapor, along with other trace species. We estimate a partial pressure of water vapor $\sim 3 \times 10^{-2}$ bar and a partial pressure of Na vapor $\sim 2 \times 10^{-5}$ bar at the boundary region through which chondrules traverse. The partial pressure of water is consistent with the abundance of fayalite in chondrules (Fedkin & Grossman 2006) and indicators of variable oxygen fugacity in the chondrule formation environment (Krot et al. 2000).

The high partial pressures of Na may resolve the mystery of how olivines crystallized form chondrule melts were able to incorporate substantial Na (Alexander et al. 2008).

We find that for plausibleinitial eccentricities ($e_0 \gtrsim 0.2$) and inclinations ($i_0 \approx 0^\circ$–15°) following a scattering event, the velocity of the planetary embryo with respect to the gas, and the speed of the bow shock, are sufficient to melt chondrules and to continue to melt chondrules over the eccentricity damping timescale. For typical chondrule-forming parameters we estimate damping timescales $\sim 10^5$ years.

Chondrules may be a byproduct of planet formation, not a necessary step toward planet formation. Chondrule formation is likely to be delayed, perhaps by 2 Myr, until the first large planetary embryos are formed and scattered. Once such bodies form, several planetary embryos can potentially melt chondrules over a span of several Myr, each one for ~ 0.1 Myr at a time. The mass of chondrules processed by a single eccentric planetary embryo is potentially as high as the entire mass of chondrules inferred to exist in the asteroid belt today, $\sim 2 \times 10^{24}$ g (Grossman 1988). A small number of planetary embryos forming chondrules intermittently over several Myr would be consistent with the ages of chondrules (Kurahashi et al. 2008; Villeneuve et al. 2009). A diversity of chondrule sizes, compositions, and textural types could result from the evolution of the solar nebula between chondrule-forming events involving protoplanets with different a, e_0, and i_0.

Yet another consideration is what type of object might be produced outside of the impact parameter necessary to produce chondrules. It is likely that solids will be fully or partially melted in these regions, and experience rapid cooling rates, resulting in objects that do not fit the classical definition of chondrules. For example, Miura et al. (2010) proposed that silicate crystals found in meteorites could be produced by supercooling of a silicate vapor in bow shocks. Alexander et al. (2007) found that the microstructure of pyroxene in interplanetary dust particles (IDPs) indicates that it formed at temperatures >1258 K and cooled relatively rapidly (~ 1000 K hr^{-1}), suggesting some type of shock heating. Scott & Krot (2005) proposed that most matrix silicates likely formed as condensates close to chondrules in transient heating events, cooling below 1300 K at ~ 1000 K hr^{-1}. Wasson & Rubin (2003) suggest that ferran olivine overgrowths on chondrules and chondrule fragments are produced by cooling rates orders of magnitude greater than those experienced by the chondrules themselves. Formation outside the chondrule-forming impact parameter in a planetary embryo bow shock may explain objects such as the silicates found in meteorites (Scott & Krot 2005; Miura et al. 2010), pyroxene in IDPs (Alexander et al. 2007), and overgrowths on chondrules (Wasson & Rubin 2003; Wasson et al. 2003). Further detailed modeling of the thermal histories of objects formed in bow shocks around planetary embryos is necessary to address this intriguing possibility.

Finally, we speculate that there is also likely to be a critical size for a body that produces chondrules with the proper thermal histories, which are not subsequently accreted. Based on the standoff distances found for the two bodies considered in this study (Section 3), we anticipate that this critical size is ~ 1000 km in radius. In future work, we plan a parameter study of bodies ranging in size from radii of 500–2720 km in order to test this hypothesis.

In this study, we have found that chondrule formation in planetary embryo bow shocks is fundamentally different from formation in planetesimal bow shocks, but on the basis of

our preliminary calculations this model appears to fit all the known constraints on chondrule formation. We intend to further develop the model, especially to include fully 2D radiative transfer in determining chondrule thermal histories, to better test whether chondrules could form in planetary bow shocks and what other types of object may form along with them. We intend to determine the critical size of a body that is necessary for chondrule formation in bow shocks. At the same time, we do not exclude other formation mechanisms for chondrules. Chondrules in CH/CB chondrites, in particular, appear to have formed from an impact plume (Krot et al. 2005). Large-scale shocks driven by gravitational instabilities also remain a viable option for chondrule formation (Morris & Desch 2010). Nevertheless, although there are some details that need to be explored further, the overall ability of the model to match chondrule constraints—especially the elevated partial pressures of volatiles—makes the planetary embryo bow shock model a very promising mechanism for chondrule formation.

REFERENCES

Adachi, I., Hayashi, C., & Nakazawa, K. 1976, Prog. Theor. Phys., 56, 1756
Alexander, C. M. O., Boss, A. P., Keller, L. P., Nuth, J. A., & Weinberger, A. 2007, in Protostars and Planets V, ed. B. Reipurth, D. Jewitt, & K. Keil (Tucson, AZ: Univ. Arizona Press), 801
Alexander, C. M. O., Grossman, J. N., Ebel, D. S., & Ciesla, F. J. 2008, Science, 320, 1617
Bitsch, B., & Kley, W. 2010, A&A, 523, 30
Bitsch, B., & Kley, W. 2011, A&A, 530, A41
Boss, A. P., & Durisen, R. H. 2005, ApJ, 621, L137
Boley, A. C., & Durisen, R. H. 2008, ApJ, 685, 1193
Chambers, J. E. 2001, Icarus, 152, 205
Chambers, J. E., & Wetherill, G. W. 1998, Icarus, 136, 304
Ciesla, F. J., Hood, L. L., & Weidenschilling, S. J. 2004b, Meteorit. Planet. Sci, 38, 1809
Ciesla, F. J., Lauretta, D. S., & Hood, L. L. 2004a, Meteorit. Planet. Sci., 39, 531
Connolly, H. C., Jr., Desch, S. J., Ash, R. D., & Jones, R. H. 2006, in Meteorites and the Early Solar System II, ed. D. S. Lauretta & H. Y. McSween, Jr. (Tucson, AZ: Univ. Arizona Press), 383
Craddock, R. A., & Greeley, R. 2009, Icarus, 204, 512
Cresswell, P., Dirksen, G., Kley, W., & Nelson, R. P. 2007, A&A, 473, 329
Cuzzi, J. N., & Alexander, C. M. O. 2006, Nature, 441, 483
Cuzzi, J. N., Dobrovolskis, A. R., & Hogan, R. C. 1996, in Chondrules and the Protoplanetary Disk, ed. R. H. Hewins, R. H. Jones, & E. R. D. Scott (Cambridge: Cambridge University Press), 35
Cuzzi, J. N., & Hogan, R. C. 2003, Icarus, 164, 127
Cuzzi, J. N., Hogan, R. C., Paque, J. M., & Dobrovolskis, A. R. 2001, ApJ, 546, 496
Dann, J. C., Holzheid, A. H., Grove, T. L., & McSween, H. Y., Jr. 2001, Meteorit. Planet. Sci., 36, 793
Dauphas, N., & Pourmand, A. 2011, Nature, 473, 489
Desch, S. J. 2007, ApJ, 671, 878
Desch, S. J., Ciesla, F. J., Hood, L. L., & Nakamoto, T. 2005, in ASP Conf. Ser. 341, Chondrites and the Protoplanetary Disk, ed. A. N. Krot, E. R. D. Scott, & B. Reipurth (San Francisco, CA: ASP), 849
Desch, S. J., & Connolly, H. C., Jr. 2002, Meteorit. Planet. Sci., 37, 183
Desch, S. J., Morris, M. A., Connolly, H. C., Jr., & Boss, A. P. 2010, ApJ, 725, 692
Desch, S. J., Morris, M. A., Connolly, H. C., Jr., & Boss, A. P. 2012, Meteorit. Planet. Sci., in press
Dubrulle, B., Morfill, G., & Sterzik, M. 1995, Icarus, 114, 237
Elkins-Tanton, L. T. 2008, Earth Planet. Sci. Lett., 271, 181
Fedkin, A. V., & Grossman, L. 2006, in Meteorites and the Early Solar System II, ed. D. S. Lauretta & H. Y. McSween, Jr. (Tucson, AZ: Univ. Arizona Press), 279
Fleming, T., & Stone, J. M. 2003, ApJ, 585, 908

Ford, E. B., & Chiang, E. I. 2007, ApJ, 661, 602
Fricker, P. E., & Reynolds, R. T. 1968, Icarus, 9, 221
Fryxell, B., Olson, K., Ricker, P., et al. 2000, ApJS, 131, 273
Furlan, E., Luhman, K. L., Espaillat, C., et al. 2011, ApJS, 195, 3
Gooding, J. L., & Keil, K. 1981, Meteoritics, 16, 17
Grimm, R. E., & McSween, H. Y. 1993, Science, 259, 653
Grossman, J. N. 1988, Nature, 334, 14
Grossman, L., Fedkin, A. V., & Simon, S. B. 2011, LPI Contributions, 1639, 9035
Hansen, B. M. S. 2009, ApJ, 703, 1131
Hartmann, L., Calvet, N., Gullbring, E., & D'Alessio, P. 1998, ApJ, 495, 385
Hayashi, C. 1981, Prog. Theor. Phys. Suppl., 70, 35
Hewins, R. H., & Connolly, H. C., Jr. 1996, in Chondrules and the Protoplanetary Disk, ed. R. H. Hewins, R. H. Jones, & E. R. D. Scott (Cambridge: Cambridge University Press), 197
Hewins, R. H., Connolly, H. C., Lofgren, G. E., Jr., & Libourel, G. 2005, in ASP Conf. Ser. 341, Chondrites and the Protoplanetary Disk, ed. A. N. Krot, E. R. D. Scott, & B. Reipurth (San Francisco, CA: ASP), 286
Holland, H. D. (ed.) 1984, The Chemical Evolution of the Atmosphere and Oceans. (Princeton, NJ: Princeton Univ. Press), 583
Hood, L. L. 1998, Meteorit. Planet. Sci., 33, 97
Hood, L. L., Ciesla, F. J., Artemieva, N. A., Marzari, F., & Weidenschilling, S. J. 2009, Meteorit. Planet. Sci., 44, 327
Hood, L. L., & Weidenschilling, S. J. 2011, in Proc. Lunar and Planetary Institute Sci. Conf. Abstracts (Houston, TX: LPI), 42, 2068
Kring, D. A. 1991, Earth Planet. Sci. Lett., 105, 65
Krot, A. N., Amelin, Y., Cassen, P., & Meibom, A. 2005, Nature, 436, 989
Krot, A. N., Fegley, B., Jr., Lodders, K., & Palme, H. 2000, in Protostars and Planets IV, ed. V. Mannings, A. P. Boss, & S. S. S. Russell (Tucson, AZ: Univ. Arizona Press), 1019
Kurahashi, E., Kita, N. T., Nagahara, H., & Morishita, Y. 2008, Geochim. Cosmochim. Acta, 72, 3865
Lauretta, D. S., Nagahara, H., & Alexander, C. M. O. 2006, in Meteorites and the Early Solar System II, ed. D. S. Lauretta & H. Y. McSween, Jr. (Tucson, AZ: Univ. Arizona Press), 431
Li, A., & Greenberg, J. M. 1997, A&A, 323, 566
Lodders, K. 2003, ApJ, 591, 1220
McCubbin, F. M., & Elardo, S. M. 2011, Lunar and Planetary Institute Science Conference Abstracts, 42, 2358
McSween, H. Y., Grove, T. L., Lentz, R. C. F., et al. 2001, Nature, 409, 487
McSween, H. Y., & Harvey, R. P. 1993, Science, 259, 1890
Miura, H., Tanaka, K. K., Yamamoto, T., et al. 2010, ApJ, 719, 642
Morris, M. A., & Desch, S. J. 2010, ApJ, 722, 1474
Morris, M. A., & Desch, S. J. 2012, Meteorit. Planet. Sci, in press
Morris, M. A., Desch, S. J., & Ciesla, F. J. 2009, ApJ, 691, 320
Morris, M. A., Desch, S. J., & Ciesla, F. J. 2010a, in Proc. Lunar and Planetary Institute Sci. Conf. Abstracts, (Houston, TX: LPI), 41, 2393
Morris, M. A., Desch, S. J., & Ciesla, F. J. 2010b, Meteorit. Planet. Sci. Suppl., 73, 5215
Mottl, M., Glazer, B., Kaiser, R., & Meech, K. 2007, Chem. Erde/Geochemistry, 67, 253
Nimmo, F., & Kleine, T. 2007, Icarus, 191, 497
Ouellette, N., Desch, S. J., & Hester, J. J. 2007, ApJ, 662, 1268
Paardekooper, S.-J. 2007, A&A, 462, 355
Paardekooper, S.-J., & Mellema, G. 2006, A&A, 459, L17
Papaloizou, J. C. B., & Larwood, J. D. 2000, MNRAS, 315, 823
Probstein, R. F. 1968, in Problems of Hydrodynamics and Continuum Mechanics, ed. M. A. Lavrentev (Philadelphia, PA: Society for Industrial and Applied Mathematics), 568
Raymond, S. N., Quinn, T., & Lunine, J. I. 2006, Icarus, 183, 265
Scott, E. R. D., & Krot, A. N. 2005, ApJ, 623, 571
Stolper, E., & Holloway, J. R. 1988, Earth Planet. Sci. Lett., 87, 397
Tanaka, H., & Ward, W. R. 2004, ApJ, 602, 388
Turner, N. J., Carballido, A., & Sano, T. 2010, ApJ, 708, 188
Van Limpt, J., Beerkens, R., & Verheijen, O. 2006, Journal of the American Ceramic Society, 89, 3446
Villeneuve, J., Chaussidon, M., & Libourel, G. 2009, Science, 325, 985
Walsh, K. J., Morbidelli, A., Raymond, S. N., O'Brien, D. P., & Mandell, A. M. 2011, Nature, 475, 206
Wasson, J. T., Kunihiro, T., & Rubin, A. E. 2003, Meteorit. Planet. Sci. Suppl., 38, 5291
Wasson, J. T., & Rubin, A. E. 2003, Geochim. Cosmochim. Acta, 67, 2239
Weidenschilling, S. J., Marzari, F., & Hood, L. L. 1998, Science, 279, 681
Weidenschilling, S. J., Spaute, D., Davis, D. R., Marzari, F., & Ohtsuki, K. 1997, Icarus, 128, 429
Wetherill, G. W., & Stewart, G. R. 1993, Icarus, 106, 190
Zahnle, K., Arndt, N., Cockell, C., et al. 2007, Space Sci. Rev., 129, 35